Research Square

Preprints are preliminary reports that have not undergone peer review.
They should not be considered conclusive, used to inform clinical practice,
or referenced by the media as validated information.

Site-Stratified Transcriptomic Integration Reveals an Immune-to- Bone-Remodeling Transition from Day 3 to Day 7 and a Conserved Core of Osteoblast–Osteoclast Coupling across Anatomical Sites in Human Alveolar Bone Osseointegration

Hanqi Su
Beijing CRS Medical Device Co., Ltd
Junjiang Hao
Haojunjiang@caresimplant.com

Beijing CRS Medical Device Co., Ltd
Yibo Liu
Stomatology College of Jiamusi University, Jiamusi University
Yifan Yin
Stomatology College of Jiamusi University, Jiamusi University
Yucheng Su
Dental Implant Center, Peking Union Medical College Hospital, Chinese Academy of Medical Sciences

Research Article

Keywords: implant osseointegration, alveolar bone, site stratification, immune-to-bone-remodeling transition, osteoblast–osteoclast coupling, cross-site conservation, hub genes

Posted Date: November 26th, 2026

DOI: https://doi.org/10.21203/rs.3.rs-11424742/v1

License: This work is licensed under a Creative Commons Attribution 4.0 International License.
Read Full License

Additional Declarations: No competing interests reported.

Site-Stratified Transcriptomic Integration Reveals an Immune-to-Bone-Remodeling Transition from Day 3 to Day 7 and a Conserved Core of Osteoblast–Osteoclast Coupling across Anatomical Sites in Human Alveolar Bone Osseointegration

Hanqi Su [1], Junjiang Hao [1,], Yibo Liu [2], Yifan Yin [2], Yucheng Su [2,3,4,5]*

[1] Beijing CRS Medical Device Co., Ltd., Beijing 102600, China

[2] Stomatology College of Jiamusi University, Jiamusi University, Jiamusi 154002, China

[3] Beijing Citident Hospital of Stomatology, Beijing 100032, China

[4] Beijing Implant Training College (BITC), Beijing 100032, China

[5] Dental Implant Center, Peking Union Medical College Hospital, Chinese Academy of Medical Sciences, Beijing 100032, China

Corresponding author: Junjiang Hao

Address: No. 2 Qingli Road, Lixian Town, Daxing District, Beijing 102604, P.R. China

Email: Haojunjiang@caresimplant.com

Author contributions

Hanqi Su: Conceptualization, Methodology, Software, Writing-Original draft preparation;

Junjiang Hao: Data curation, Writing-Reviewing and Editing;

Yibo Liu: Software, Visualization, Writing-Reviewing and Editing;

Yifan Yin: Visualization, Writing-Reviewing and Editing

Hanqi Su: Funding acquisition, Supervision, Writing-Reviewing and Editing.

Yucheng Su: Conceptualization, Writing-Reviewing and Editing;

Abstract

Background: Longitudinal transcriptomic evidence on implant osseointegration has largely been derived from long-bone implantation models. Whether human alveolar bone exhibits a reproducible immune-to-bone-remodeling transcriptional transition, and whether a core program of osteoblast–osteoclast coupling is conserved across anatomical sites and species, remain insufficiently characterized using oral data. This study aimed to identify early transcriptional changes in human alveolar bone and evaluate their cross-site and cross-species conservation.

Methods: A site-stratified transcriptomic integration strategy was adopted. The human alveolar bone dataset GSE41446, comprising 44 samples from 11 participants, two implant surfaces, and day 3 (D3) and day 7 (D7), served as the core discovery dataset. Rat maxillary bone dataset GSE304968 and rat tibial and femoral datasets were used for cross-site comparisons. Analyses included differential expression analysis, directional validation paired by participant and implant surface, weighted gene co-expression network analysis (WGCNA), robust rank aggregation, and machine-

learning feature selection. A rat tibial osseointegration time series (GSE35976) was further used to assess the cross-species directional concordance of candidate hub genes.

Results: From D3 to D7, the reparative macrophage marker MRC1 was upregulated, whereas the inflammatory genes TNF and IL1B were downregulated. Genes involved in osteogenesis–extracellular matrix (ECM) processes and osteoclast-mediated matrix remodeling, including CTSK, COL1A1, COL3A1, SPARC, LOX, and ALPL, were coordinately upregulated, supporting a transcriptional transition from an inflammation-dominated state toward repair and bone remodeling. Directional single-sample gene set enrichment analysis (ssGSEA) showed increased enrichment scores for the reparative macrophage gene set in 19 of 22 paired samples. The magnitude of this change exceeded the empirical distribution of random 10-gene sets analyzed in the same run ($P = 0.017$), although this result was considered exploratory because of the limited number of random sets. Cross-site classification identified 42 directionally concordant conserved genes that were significantly enriched for osteogenesis (fold enrichment [FE] = 73.3, $P = 7.1 \times 10^{-13}$). The human WGCNA red module contained 159 genes and showed a preservation proportion of 64.6% among genes detectable on the rat platform, significantly exceeding the random baseline of 34.2% (hypergeometric $P = 1.77 \times 10^{-11}$; modulePreservation Zsummary = 13.31). Machine-learning analysis identified 11 candidate hub genes. CTSK, which received five of five selection votes, was upregulated in both human alveolar bone and the early rat tibial time series. Nested cross-validation, with feature selection performed within the training folds, yielded an area under the receiver operating characteristic curve (AUC) of 0.980 ± 0.045. By comparison, 10,000 random 11-gene signatures achieved a mean macro-averaged F1 score (Macro-F1) of 0.724 ± 0.085, indicating strong global time-associated transcriptional separation between D3 and D7. Oral-specific genes were primarily enriched for translation and mitochondrial energy metabolism, providing no evidence for a distinct oral-specific osseointegration pathway.

Conclusions: Human alveolar bone exhibits an immune-to-bone-remodeling transcriptional transition from D3 to D7. A core program coupling osteogenesis–ECM processes with osteoclast-mediated matrix remodeling shows directional concordance between oral and orthopedic datasets. CTSK represents a priority candidate process biomarker for further validation. Because these findings are hypothesis-generating observations derived from a single human cohort, independent human alveolar bone samples, protein quantification, and functional experiments are required before clinical translation can be considered.

Keywords: **implant osseointegration; alveolar bone; site stratification; immune-to-bone-remodeling transition; osteoblast–osteoclast coupling; cross-site conservation; hub genes**

1. Introduction

Implant osseointegration provides the biological foundation for the long-term success of dental implant rehabilitation and has been reconceptualized as a dynamic process of osteoimmunomodulation at the interface with a persistent foreign body [1-4]. Unlike long-bone implants, dental implants encounter distinct biological challenges within the alveolar bone environment. Alveolar bone undergoes continuous functional adaptive remodeling regulated by dentition-related loading and the oral microenvironment. Its developmental origin, regulation of osteoblast lineages, and vascularization patterns differ systematically from those of mesoderm-derived long bones formed through endochondral ossification [5]. In addition, the oral mucosal barrier, salivary microenvironment, and persistent microbial exposure increase susceptibility to interface infection and peri-implant diseases [6-9]. These site-specific factors suggest that the molecular programs underlying dental implant osseointegration cannot readily be extrapolated from orthopedic implantation models. Nevertheless, the available transcriptomic evidence on osseointegration remains dominated by orthopedic models involving the tibia and femur, with very limited oral bone sample sizes and coverage of early healing. Whether molecular programs at the alveolar bone site can be directly characterized by transcriptomics therefore remains unresolved.

Anatomical and developmental evidence likewise supports substantive differences between alveolar and long bones during osseointegration. Alveolar bone originates from neural crest-derived ectomesenchyme and forms through intramembranous ossification, whereas long bones originate from the mesoderm and undergo endochondral ossification [10]. The two also differ in osteoblast lineage regulation, vascularization patterns, and mechanical load transmission [11-13]. Clinical evidence indicates that peri-implant crestal bone remodeling in alveolar bone differs markedly from stress-adaptive remodeling in long-bone cortical tissue [14]. Implant surface chemistry and micro/nanotopography can substantially alter interfacial osseointegration [15, 16]. However, systematic molecular evidence is lacking as to whether these surface effects amplify or reshape oral site-specific transcriptional programs. Although core programs governing osteogenic differentiation, including RUNX2/SP7/ALPL, are conserved throughout the skeletal system [17], systematic transcriptomic evidence derived from oral datasets remains insufficient to establish oral-specific features of immune–bone-remodeling coupling.

Research on bone–immune coupling has established macrophage polarization as a key component of osseointegration and fracture healing [18-22]. Moderate inflammation early after implantation facilitates necrotic tissue clearance and chemokine release. A timely subsequent transition toward reparative, M2-like macrophages promotes vascularization and maturation of the osteogenic microenvironment through paracrine factors such as transforming growth factor beta

(TGF-β) and vascular endothelial growth factor (VEGF) [23]. Single-cell studies of implant interfaces further support a central role for macrophage subsets in remodeling the immune-inflammatory microenvironment [24, 25]. However, much of this evidence comes from animal models or sampling at a single time point, making it difficult to directly characterize the timing of the transition from inflammation resolution to the initiation of bone remodeling in human alveolar bone osseointegration. In vivo human assessments also predominantly involve histological and imaging examinations at later stages of osseointegration [25, 26], with very limited transcriptomic characterization of the early window extending from several days to two weeks after surgery [27].

Against this background, we addressed three interrelated questions: whether human alveolar bone exhibits reproducible immune–bone-remodeling transcriptional changes from day 3 (D3) to day 7 (D7); which osteogenesis–extracellular matrix (ECM) programs remain concordant between oral and orthopedic datasets; and whether candidate hub genes with evidence of cross-site relevance can be identified from oral data.

To address these questions, oral bone datasets served as the basis for core discovery, whereas tibial and femoral datasets were used only for cross-site comparisons. Candidate hub genes were further assessed for cross-species conservation using a rat tibial time series. The analytical workflow comprised differential expression analysis, weighted gene co-expression network analysis (WGCNA), robust ranking, and machine-learning feature selection.

2. Materials and Methods

2.1 Study design and dataset stratification

We adopted a site-stratified strategy for integrating public transcriptomic datasets. Datasets were assigned a priori to an oral bone stratum (core discovery) or an orthopedic reference stratum (cross-site comparison), and the evidential scope of the conclusions was defined accordingly. Oral datasets generated the core findings, whereas orthopedic datasets were used only to evaluate cross-site conservation and did not substitute for independent validation in human alveolar bone. In addition to this stratification, immune directional validation was performed in the core human alveolar bone dataset, GSE41446 [26]. Each dataset was stratified according to the time points, participants, implant surfaces, treatment conditions, and pairing relationships recorded in its original metadata. GSE41446 has a within-participant paired structure, with each participant contributing samples from two implant surfaces at two time points. This structure was used for participant-by-surface paired testing in immune directional validation; the primary differential expression analysis used between-group comparisons. Temporal comparisons were restricted to time points

shared by and unambiguously identifiable in the original data. Datasets that could not be traced or lacked essential metadata were excluded from all analyses.

2.2 Data retrieval and inclusion

Dataset searches were completed on August 5, 2026, through the Gene Expression Omnibus (GEO), using the GEO DataSets (GDS) interface, and the Sequence Read Archive (SRA), following the record-keeping framework of the Preferred Reporting Items for Systematic Reviews and Meta-Analyses (PRISMA) 2020 statement [28]. Search terms covered oral implantation (dental/oral/tooth/alveolar/maxillary/mandibular implant combined with osseointegration, peri-implant bone, bone-implant interface, and related terms), orthopedic implantation comparators (orthopedic implant, bone screw, tibial/femoral implant, and intramedullary combined with osseointegration), and broader supplementary searches for osseointegration expression profiles. Searches were restricted to “Expression profiling by array” or “Expression profiling by high throughput sequencing.” After deduplication, 36 candidate datasets were identified and manually reviewed for tissue source, implantation site, species, experimental design, time points or treatment conditions, sample information, and data traceability. Inclusion required a clearly defined osseointegration- or implant-related experimental context, availability of expression matrices or raw data, and sufficient metadata to reconstruct the prespecified comparisons. Datasets with unclear provenance, untraceable records, or unsuitable comparison conditions were excluded.

2.3 Data preprocessing and harmonization of gene symbols

Raw Affymetrix HuGene 1.1 ST CEL files from GSE41446 were processed using the oligo workflow in R and normalized using robust multi-array average (RMA). Transcript clusters were mapped to gene symbols using hugene11sttranscriptcluster.db, with original identifiers retained for unmapped entries. Other microarray datasets used platform-normalized log2 expression values. For RNA sequencing (RNA-seq) datasets, the officially provided expression matrices were used: transcripts per million (TPM) for GSE304968 [29], fragments per kilobase of transcript per million mapped reads (FPKM) for GSE113520, and raw counts for GSE227869 [30]. Following platform-specific normalization or expression transformation within each dataset, datasets were integrated through a unified gene-symbol mapping table. Rat and mouse gene symbols were converted to their corresponding human ortholog symbols. When multiple microarray transcript clusters mapped to the same gene, the maximum expression value was retained. All cross-dataset comparisons were conducted at the harmonized gene-symbol level.

2.4 Differential expression analysis

Prespecified comparisons were established according to each dataset's original experimental design: D7 versus D3 in human alveolar bone for GSE41446; loading versus no loading in rat maxillary bone for GSE304968; D4 versus D2 in rat tibia for GSE35976 [31]; lithium-treated day 7 (Li-D7) versus control day 7 (Ctrl-D7) in rat tibia for GSE54294 [32]; hyperlipidemia treatment versus control in rat femur for GSE113520; and sorted leptin receptor-positive ($LEPR^+$) versus lineage-negative (Lin^-) cells in mouse tibia for GSE227869. Genes with mean log2 expression below 1 in both groups were removed before analysis. Platform-normalized log2 expression values were used for the microarray datasets (GSE41446, GSE35976, and GSE54294). RNA-seq values (TPM in GSE304968, FPKM in GSE113520, and raw counts in GSE227869) were transformed using $\log2(x + 1)$. Between-group differences in means were assessed using two-sided Welch's t-tests with unequal variances, yielding log2 fold changes (log2FC), raw P values, and Benjamini–Hochberg (BH)-adjusted false discovery rates (FDRs). The same significance thresholds were applied to all datasets: FDR < 0.05 and $|\log2FC| \geq 0.5$. Because GSE41446 has a fully crossed design involving 11 participants, each contributing two surfaces × two time points, the time effect was additionally assessed using log-linear models with participant fixed effects. The model Y ~ C(subject) + surface + day evaluated the main effects of day and surface, and the model Y ~ C(subject) + surface + day + surface:day evaluated the day-by-surface interaction. Two surface-stratified within-participant paired models, Y ~ C(subject) + day (22 samples each), evaluated D3-to-D7 changes separately for Osseospeed and TiOblast. Significance in the paired models likewise required $|\text{coefficient}| \geq 0.5$ and FDR < 0.05.

2.5 Cross-site conservation classification and cross-site validation of hub genes

Significantly differentially expressed genes were pooled separately within the oral stratum (GSE41446 and GSE304968) and the orthopedic stratum (GSE35976, GSE54294, and GSE113520), then cross-classified using harmonized gene symbols and the prespecified significance thresholds. Conserved genes were defined as significant in both strata with concordant directions of the mean expression effects within strata; Oral-specific genes were significant only in the oral stratum, or significant in both strata with opposite directions; and Ortho-specific genes were significant only in the orthopedic stratum. Because comparisons across datasets could represent temporal, loading, or treatment effects, this classification was treated as a descriptive site comparison rather than an estimate of effects under an identical biological stimulus. GSE227869 was used only for differential expression analysis and directional reference for key genes and was excluded from pooled cross-site classification. Each category was further analyzed for

enrichment in curated gene sets representing osteogenesis, fibrosis, remodeling, and immunity, as well as Gene Ontology (GO) terms. Cross-site conservation of candidate hub genes was evaluated in the orthopedic datasets using the same rules. The rat tibial time series (GSE35976) was used to assess candidate gene directionality during early osseointegration, and the rat femoral model (GSE113520) provided supplementary comparisons. Priority was given to platforms capable of detecting the corresponding orthologs, and "not measurable on the platform" was recorded separately from "not significant." This step assessed cross-site and cross-species conservation and did not replace independent human alveolar bone validation.

2.6 Directional validation of immune gene sets using single-sample gene set enrichment analysis

Immune directional validation was performed in the core human alveolar bone dataset GSE41446 (44 samples; 11 participants × 2 implant surfaces × D3/D7). The probe-level log2 RMA expression matrix was mapped to gene symbols using GPL11532 annotations, retaining the maximum expression value when multiple probes mapped to the same gene. Using gseapy 1.3.0, single-sample gene set enrichment analysis (ssGSEA) scores were calculated for prespecified reparative macrophage, M1-like, and pan-inflammatory axis gene sets on a harmonized gene-by-sample matrix, and normalized enrichment scores (NES) normalized within the same run were reported. The primary D3-versus-D7 comparison used the Wilcoxon signed-rank test paired by participant and surface; the Mann–Whitney U test was used only for supplementary description. In addition, 300 random 10-gene sets were included in the same run for empirical calibration to distinguish the directionality of prespecified gene sets from global transcriptional drift. NES values were comparable only within the same run. This analysis provided directional support for immune programs and was not used to infer absolute cell proportions, cell counts, or cellular composition at single-cell resolution.

2.7 WGCNA co-expression networks and cross-species conservation

A signed co-expression network was constructed from the 5,000 most highly variable genes in human alveolar bone using the R package WGCNA (v1.74), with minModuleSize = 30, deepSplit = 2, and mergeCutHeight = 0.25 [33]. Candidate softPower values were assessed using pickSoftThreshold over powers of 4–20 in increments of 2, and softPower = 18 was selected. Sensitivity analyses examined softPower values of 10, 14, 18, and 20 and clustering parameters of minModuleSize 20/30/50 × deepSplit 1/2/3. Jaccard similarity was used to assess the robustness of module boundaries. Module functions were assessed using Fisher's exact tests for enrichment in curated gene sets. Rat datasets were analyzed using the same network construction and module identification framework to ensure cross-species comparability. Cross-species conservation was evaluated using ortholog mapping, permutations of size-

matched random gene sets as negative controls, hypergeometric tests, and WGCNA modulePreservation analysis (nPerm = 50; human modules as the reference set and rat modules as the test set) [34]. The number of permutations and conservation criteria were prespecified and recorded in the analysis scripts.

2.8 Robust rank aggregation analysis

Robust rank aggregation (RRA) was applied to integrate rankings across four datasets with complete ranked inputs (GSE41446, GSE304968, GSE35976, and GSE54294), using aggregateRanks with method = "RRA" in R [35]. Within each dataset, all genes were ranked by ascending two-sided P value. Expression direction was recorded separately according to the sign of log2FC and assigned only when at least two datasets agreed; direction was not incorporated into the ranking statistic. Gene symbols were harmonized and duplicate entries resolved before analysis. This analysis evaluated the cross-dataset ranking significance of prespecified key gene sets involved in osteogenesis–ECM processes and bone remodeling. Because candidate genes were selected a priori based on established skeletal biology, this was a targeted confirmatory analysis rather than an unbiased discovery analysis. Results were reported as nominal P values without correction for multiple testing and should be distinguished from independent differential expression evidence in the human data.

2.9 Machine-learning selection of hub genes

A candidate gene pool was assembled for D3-versus-D7 classification in GSE41446, incorporating differentially expressed genes from human alveolar bone, genes identified through cross-site classification, and literature-reported osseointegration candidates. Following analysis of variance (ANOVA) pre-screening, feature selection was performed using five methods: least absolute shrinkage and selection operator (LASSO), random forest, extreme gradient boosting (XGBoost), recursive feature elimination (RFE), and the ANOVA F-test. Genes selected by at least three of the five methods were designated candidate hub genes. Classification performance was evaluated using outer five-fold stratified cross-validation with a fixed random seed through two approaches: one using a prespecified fixed hub signature, and a nested approach repeating feature selection within each training fold while keeping the test fold inaccessible during feature selection. A random forest classifier with fixed parameters (n_estimators = 200) was used. To compare the candidate signature against a random baseline, fixed-signature evaluation using linear discriminant analysis (LDA) and the same five-fold splits was repeated for 10,000 length-matched random 11-gene signatures, with empirical P values calculated from the macro-averaged F1 score (Macro-F1). SHapley Additive exPlanations (SHAP),

implemented with TreeExplainer, were also used to assess feature contributions in XGBoost and random forest models. All machine-learning results were considered hypothesis-generating analyses within a single cohort.

2.10 Grading literature-based functional evidence for hub genes

The known bone-related functions of each candidate hub gene were reviewed. PubMed queries combined bone-related terms, including osteoclast, osteoblast, bone resorption, and bone regeneration, with functional-evidence terms such as knockout, deficient, and in vivo. Only PubMed identifiers (PMIDs) and bibliographic information verified against search results were recorded. Evidence was graded according to prespecified criteria: L1, functional knockout or in vivo bone phenotype evidence; L2, in vitro differentiation, functional, or protein evidence without an in vivo bone phenotype under healthy physiological conditions; L3, expression, immunolocalization, or general marker associations; and L4, no direct bone evidence, with interpretation based only on annotation or protein-family inference. The primary functional cell type, supporting reference, and evidential limitations were recorded for each gene.

2.11 Statistical analysis and visualization

Statistical analyses were performed in Python (numpy, pandas, scipy, scikit-learn, xgboost, and gseapy 1.3.0) and R (WGCNA v1.74, RobustRankAggreg, oligo, and sva). Primary differential expression screening used two-sided Welch's t-tests with unequal variances, followed by reassessment of the time effect using linear models with participant fixed effects. For ssGSEA immune axes, the primary comparison used the Wilcoxon signed-rank test paired by participant and surface, with the Mann–Whitney U test as a supplementary analysis. Other two-group comparisons, such as comparisons of hub genes in validation datasets, used the Mann–Whitney U test. Multiple testing was controlled using the BH procedure [36]. Gene set enrichment was assessed using hypergeometric tests or Fisher's exact tests with BH correction. Empirical P values for permutation tests were calculated as (number of permutations at least as extreme as the observed result + 1)/(total number of permutations + 1). Principal component analysis (PCA) was used to assess the contributions of time, surface, and participant to overall expression variation. Surrogate variable analysis (SVA) was used to estimate latent surrogate variables and their associations with the main experimental factors [37]. Quality control also examined scanning dates, sample outliers, and batch information.

3. Results

3.1 Dataset overview and site stratification

A renewed search restricted to oral sites confirmed the scarcity of oral bone transcriptomic datasets. The Core Discovery stratum contained only two oral bone datasets: GSE41446 from human alveolar bone (n = 44; 11 participants × 2 surfaces × D3/D7) and GSE304968 from rat maxillary bone (n = 12; loading/no loading). Four orthopedic datasets, comprising three tibial datasets and one femoral dataset, served as cross-site references. Cross-site conservation of candidate hub genes was validated using a rat tibial osseointegration time series (GSE35976, D2/D4; Table 1). Verification of the original metadata confirmed that GSE41446 included only D3 and D7 (n = 22 each); all temporal analyses therefore concerned the D3-to-D7 interval. SCP1329, a tibial single-cell dataset, was found to be untraceable and was excluded entirely. Quality control showed that the first principal component (PC1) explained 30.0% of the variance and correlated with day (r = 0.68). D3 and D7 separated along PC1, whereas implant surface did not produce clear separation. SVA estimated six surrogate variables; the correlation between the first surrogate variable (SV1) and day reflected global transcriptional changes dominated by time. No strong batch confounding independent of time and surface was observed. Scanning dates were consistent, and no sample outliers were identified (Fig. 1).

Table 1. Dataset inclusion and stratification.

Stratum	Dataset	Species / Tissue	Sample Size	Site Category	Role
Core Discovery	GSE41446	Human / Alveolar bone	N=44	Oral bone	Primary discovery
Core Discovery	GSE304968	Rat / Maxillary bone	N=12	Oral bone	Supporting discovery
Cross-site	GSE35976	Rat / Tibia	N=16	Orthopedic bone	Cross-site comparison
	GSE54294		N=24		
Cross-site	GSE113520	Rat / Femur	N=8	Orthopedic bone	Cross-site comparison
Cross-site	GSE227869	Mouse / Tibia	N=13	Orthopedic bone	Cross-site comparison

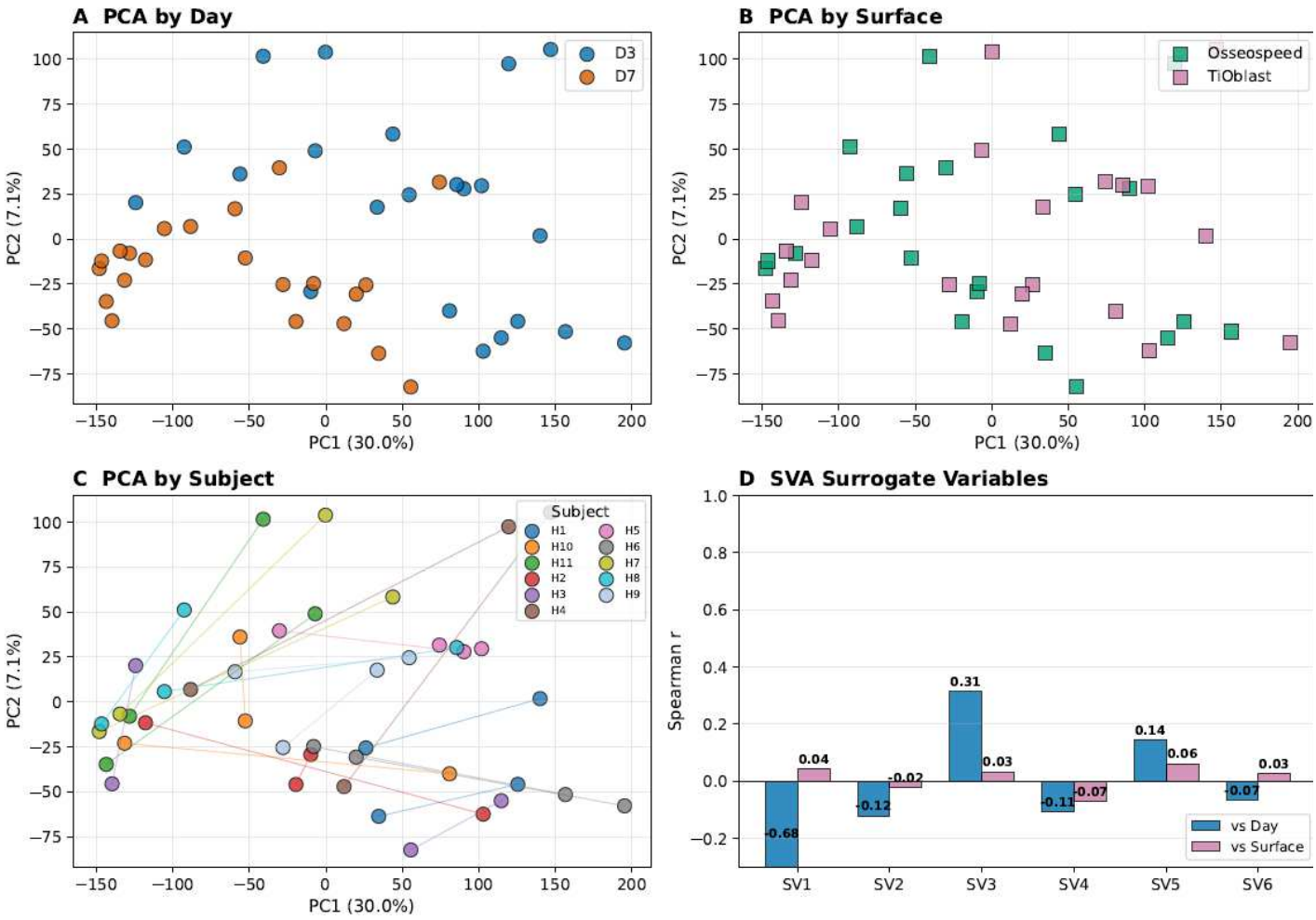

Figure 1. Global expression quality control and surrogate variable assessment in GSE41446.

A: Principal component analysis (PCA) colored by time point.

B: PCA colored by implant surface.

C: Correlation between the first principal component (PC1) and day.

D: Surrogate variable analysis (SVA) and correlations with major experimental factors.

3.2 The immune-to-bone-remodeling transition, cross-site classification, and functional enrichment in human alveolar bone

In the human alveolar bone dataset GSE41446, genes involved in osteogenesis–ECM processes and bone remodeling were broadly upregulated from D3 to D7, whereas inflammation-related genes were downregulated. CTSK, COL3A1, COL1A1, SPARC, LOX, MMP12, and ALPL were all upregulated at D7, with CTSK showing the largest change (log2FC = +3.66). The reparative macrophage marker MRC1 was upregulated (log2FC = +1.09), whereas the inflammation-related genes IL1B and TNF were downregulated (log2FC = −1.67 and −0.61, respectively). CD163 and IL6 did not meet the multiple-testing-adjusted significance criteria (FDR = 0.083 and 0.201, respectively; Fig. 2A).

Cross-classification according to significance and expression direction in the oral and orthopedic strata identified 42 Conserved, 4,359 Oral-specific, and 436 Ortho-specific genes (Fig. 2C). The significant gene pools in both strata were driven primarily by early time-series comparisons. Conserved genes were enriched for osteogenesis, ECM, and remodeling programs (osteogenesis fold enrichment [FE] = 73.3, P = 7.1×10^{-13}; Fig. 2B). Oral-specific genes showed no significant enrichment in the curated osteogenesis, fibrosis, remodeling, or immune gene sets, but were enriched in pathways related to translation, oxidative phosphorylation, the tricarboxylic acid (TCA) cycle, and mitochondrial adenosine triphosphate (ATP) synthesis (Fig. 2D).

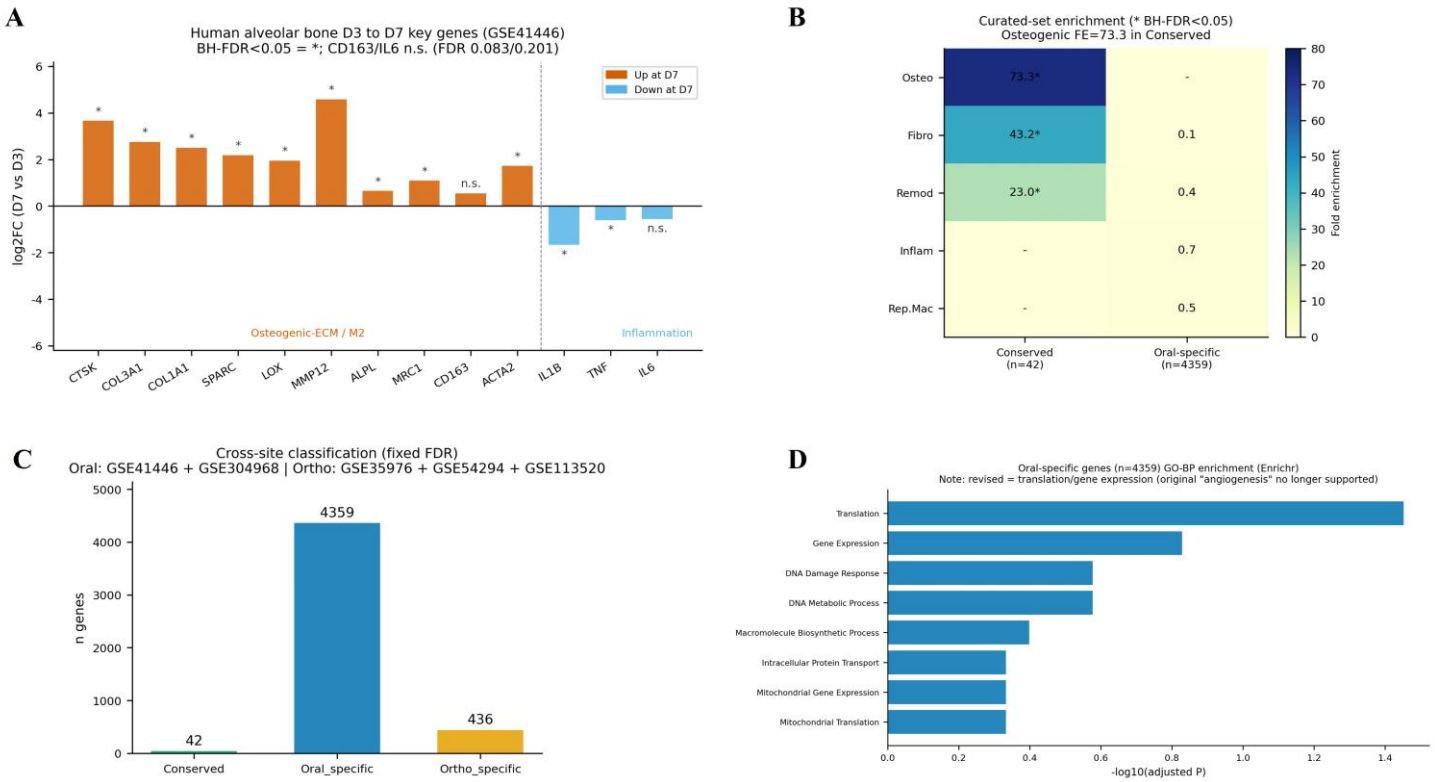

Figure 2. Immune-to-bone-remodeling transition and cross-site classification in human alveolar bone from D3 to D7
A: Principal component analysis (PCA) colored by time point. Paired-model effect sizesof key genes
B: Curated enrichment heatmap of Conserved and Oral-specific genes
C: Counts of genes in each cross-site category
D: GO enrichment of Oral-specific genes

For immune directional validation, ssGSEA in GSE41446 (Fig. 3) showed an overall increase in the reparative macrophage gene set at D7 relative to D3 (ΔNES = +0.104; increases in 19 of 22 pairs), whereas the M1-like and pan-inflammatory axes generally decreased (decreases in 16 and 15 of 22 pairs, respectively). Calibration against 300 random 10-gene sets analyzed in the same run showed that the magnitude of the reparative macrophage change exceeded random expectation (two-sided empirical P = 0.017). Although the M1-like and pan-inflammatory axes changed in the expected direction, their magnitudes did not exceed the random-set distribution. Given the extensive

global transcriptional reprogramming from D3 to D7, nominal paired P values for ssGSEA scores cannot alone establish gene-set-specific evidence. These findings therefore provide directional support consistent with MRC1 upregulation and TNF/IL1B downregulation, rather than independent confirmation.

Because GSE41446 has a fully crossed design involving 11 participants, with each participant contributing samples from two implant surfaces at D3 and D7, we reassessed the time effect using participant fixed-effects models. In the model $Y \sim C(\text{subject}) + \text{surface} + \text{day}$, using $|\text{coefficient}| \geq 0.5$ and FDR < 0.05 as the significance criteria, the day main effect identified 4,537 genes (3,167 upregulated and 1,370 downregulated). Neither the surface main effect nor the day-by-surface interaction identified any significant genes (0 for each), suggesting directionally concordant D3-to-D7 transcriptional dynamics across the two surfaces and a limited transcriptional influence of surface within this interval. Surface-stratified within-participant paired models identified 2,159 and 4,217 probes with significant D3-to-D7 changes for Osseospeed and TiOblast, respectively, with highly concordant directions. The paired models closely agreed with the primary unpaired Welch's t-test analysis: the correlation between day coefficients and unpaired log2FC values was r = 1.000, and the P-value correlation was r = 0.9937. Thus, explicitly modeling the paired structure did not alter effect directions or significance rankings, supporting the robustness of the primary findings. In a balanced fully crossed design, however, the point estimate of the day main effect is mathematically equal to the unpaired between-group mean difference; an effect-size correlation near 1 is therefore expected. The main benefit of paired modeling is more accurate estimation of variance and significance, rather than a change in effect size itself.

Among 17 prespecified key genes, 16 showed concordant paired directions across the two surfaces (Table 2). Paired effect estimates were CTSK +3.661 (FDR = 1.3×10^{-11}; +3.581 within Osseospeed and +3.741 within TiOblast), COL3A1 +2.753, COL1A1 +2.505, SPARC +2.187, LOX +1.950, ACTA2 +1.720, MRC1 +1.089 (FDR = 2.1×10^{-4}), and ALPL +0.651, together with downregulation of IL1B (−1.669) and TNF (−0.607). CD163 (+0.546, FDR = 0.093) and IL6 (−0.560, FDR = 0.056) did not reach adjusted significance, whereas RUNX2 (+0.491, FDR = 1.2×10^{-3}) did not meet the $|\text{coefficient}| \geq 0.5$ threshold. BMP2 showed no significant change in the human alveolar bone paired model (FDR = 0.929). Its significance in RobustRankAggreg reflects support for the prespecified osteogenic gene set at the cross-dataset ranking level. These findings concern different levels of evidence and are not contradictory.

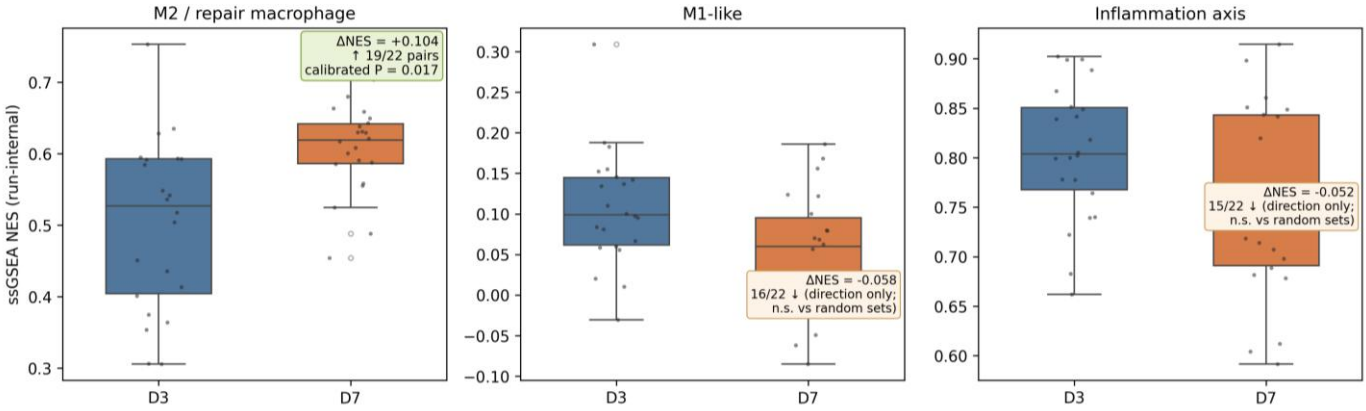

Figure 3. Directional ssGSEA validation of the D3-to-D7 immune-state transition in human alveolar bone

Table 2. Paired-model validation of key genes in human alveolar bone (GSE41446): effect sizes, surface-stratified paired changes and direction consistency

Gene	Group	Effect (D7−D3, log2)	Paired day FDR	Osseospeed paired Δ (D7−D3)	TiOblast paired Δ (D7−D3)	OS/TIO direction consistent
MRC1	Immune – repair macrophage	1.089	2.09×10^{-4}	+1.188*	+0.989*	Yes
CD163	Immune – repair macrophage	0.546	0.093 n.s.	+0.532 n.s.	+0.560 n.s.	Yes
IL6	Immune – inflammatory	−0.560	0.056 n.s.	−0.190 n.s.	−0.930*	Yes
TNF	Immune – inflammatory	−0.607	3.22×10^{-4}	−0.579*	−0.636 n.s.	Yes
IL1B	Immune – inflammatory	−1.669	1.48×10^{-5}	−1.397*	−1.942*	Yes
CTSK	Osteogenic–ECM	3.661	1.27×10^{-11}	+3.581*	+3.741*	Yes
COL3A1	Osteogenic–ECM	2.753	5.99×10^{-9}	+2.638*	+2.869*	Yes
COL1A1	Osteogenic–ECM	2.505	1.15×10^{-8}	+2.426*	+2.585*	Yes
SPARC	Osteogenic–ECM	2.187	1.09×10^{-8}	+1.969*	+2.405*	Yes
LOX	Osteogenic–ECM	1.95	9.67×10^{-6}	+1.941*	+1.958*	Yes
ACTA2	Osteogenic–ECM	1.72	3.11×10^{-10}	+1.721*	+1.719*	Yes
ALPL	Osteogenic–ECM	0.651	0.004	+0.526 n.s.	+0.776*	Yes
RUNX2	Transcription factor / other	0.491	0.001 n.s.	+0.351 n.s.	+0.631*	Yes
TWIST1	Transcription factor / other	0.242	0.074 n.s.	+0.232 n.s.	+0.253 n.s.	Yes
BMP2	Transcription factor / other	−0.010	0.929 n.s.	+0.047 n.s.	−0.068 n.s.	No
SP7	Transcription factor / other	−0.139	0.183 n.s.	−0.116 n.s.	−0.162 n.s.	Yes
VEGFA	Transcription factor / other	−1.026	0.007	−0.599 n.s.	−1.454*	Yes

OS = Osseospeed; TIO = TiOblast; Δ = D7 − D3

3.3 WGCNA: the osteogenic–ECM module and cross-species conservation

The WGCNA module structure, key-gene module membership, cross-species preservation, and robust rank aggregation results are summarized in Fig. 4.

In the human alveolar bone dataset GSE41446, signed WGCNA with a soft-thresholding power of 18 identified 10 co-expression modules. Module numbers and boundaries were consistent across repeated runs with fixed parameters and a fixed random seed (Fig. 4A). Analysis of key-gene module membership identified the red module, comprising 159

genes, as the core osteogenic–ECM module. Representative genes included CTSK, COL1A1, COL3A1, LOX, SPARC, and ALPL. This module was significantly enriched for osteogenesis-related processes (fold enrichment [FE] = 31.4, FDR = 8.7×10^{-11}) and fibrosis/ECM-related processes (FE = 21.0, FDR = 2.1×10^{-5}). The magenta module showed reparative macrophage-associated features and contained MRC1, CD163, TGFB1, and FN1, whereas the green module primarily reflected inflammatory and innate immune programs, with representative genes including IL6, IL1B, and CXCL8 (Fig. 4B).

Cross-species conservation analysis showed that 113 of the 159 genes in the human red module were detectable on the rat platform. Of these, 73 belonged to the best-matching rat module, accounting for 64.6% of detectable genes and exceeding the random baseline of 34.2%. This enrichment was supported by a hypergeometric test ($P = 1.77 \times 10^{-11}$), and modulePreservation analysis also indicated strong preservation (Zsummary = 13.31; Fig. 4C). These results support substantial cross-species conservation of the osteogenic–ECM co-expression structure.(Fig. 4D)

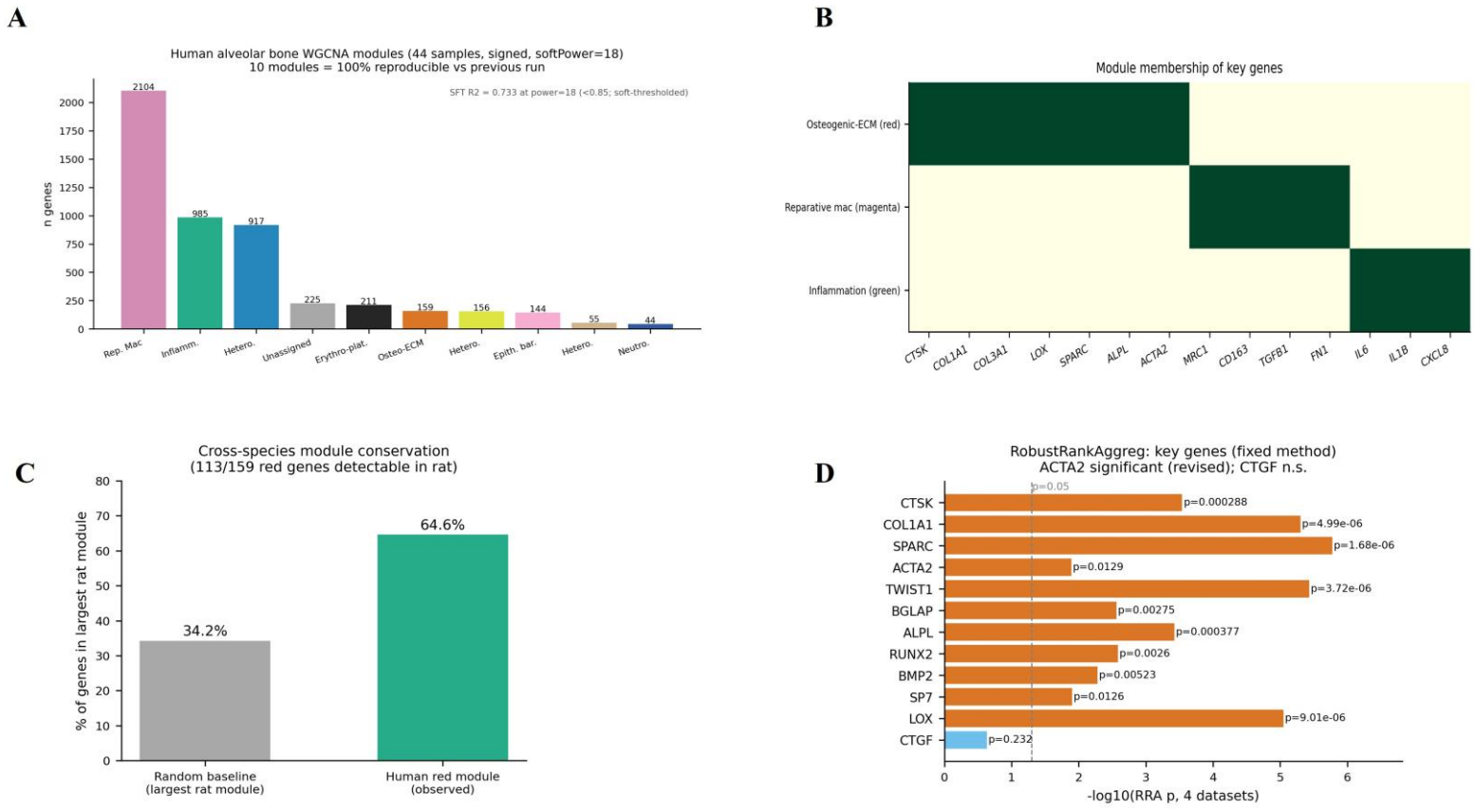

Figure 4. Construction, cross-species conservation, and robust ranking of the osteogenic–ECM co-expression module in human alveolar bone.

A: Composition and gene counts of WGCNA modules；

B: Module membership of key genes

C: Cross-species conservation of the human osteogenic–ECM (red) module ；

D: RobustRankAggreg analysis of key genes

Robust rank aggregation generated the primary ranking across four datasets using a harmonized gene pool of 45,772 genes. Supporting analyses stratified by comparison type used gene pools of 42,423 genes for time-series comparisons and 7,414 genes for loading/treatment comparisons. The expression directions of key genes were consistent between the primary and stratified analyses.

Of the 12 candidate genes evaluated by robust rank aggregation, 11 reached nominal significance ($P < 0.05$): CTSK, COL1A1, SPARC, ACTA2, TWIST1, BGLAP, ALPL, RUNX2, BMP2, SP7, and LOX. CTGF did not reach significance ($P = 0.232$; Fig. 4D). RUNX2, TWIST1, SP7, and BGLAP were not included among the prespecified 5,000 most highly variable genes in the human dataset, limiting assessment of their module membership and co-expression relationships in the human network. Co-expression signals involving osteogenic transcription factors were observed primarily in the rat data and require further validation using deeper human RNA sequencing or independent experiments.

3.4 Hub gene selection, cross-site validation, and classification performance

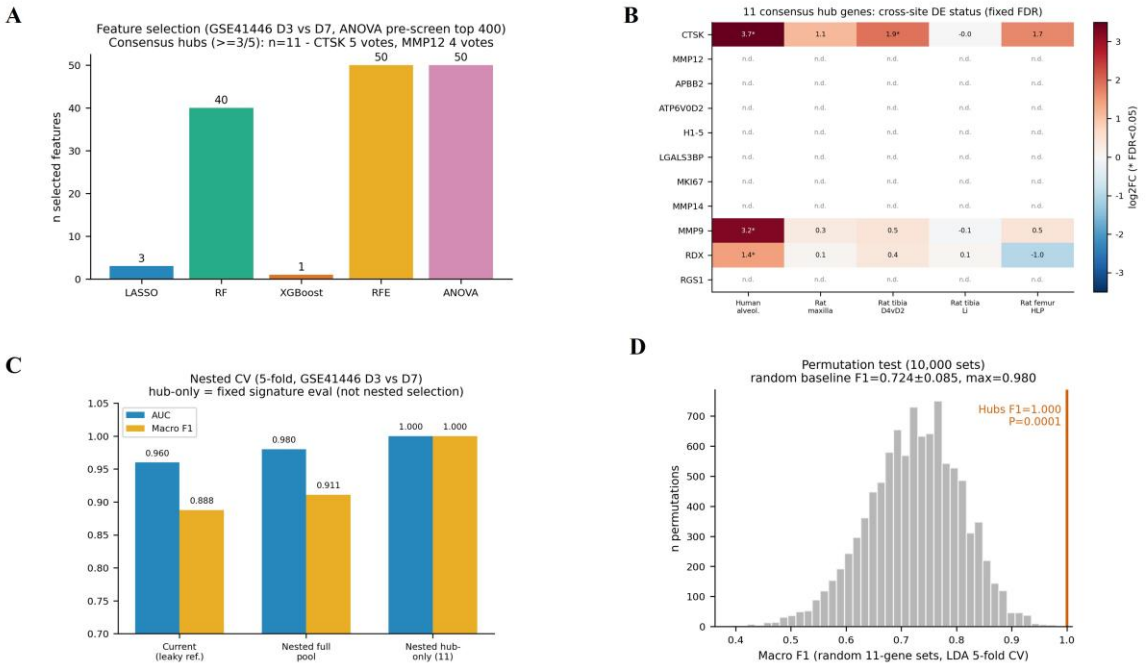

Figure 5. Hub gene selection, cross-site validation, and classification performance in human alveolar bone from D3 to D7
A: Consensus Hub gene selection across five machine-learning methods ;
B: Cross-site differential-expression status of the 11 consensus Hub genes
C: Cross-validation performance ;
D: Permutation-based assessment of F1 performance against random gene sets

For D3-versus-D7 classification in human alveolar bone dataset GSE41446, five feature-selection methods were applied: LASSO, random forest, XGBoost, RFE, and ANOVA. Genes selected by at least three of the five methods

were designated candidate hub genes (Fig. 5A). The five methods selected 3, 40, 1, 50, and 50 features, respectively, yielding 11 consensus hub genes. CTSK received 5/5 votes, MMP12 received 4/5 votes, and APBB2, ATP6V0D2, H1-5, LGALS3BP, MKI67, MMP14, MMP9, RDX, and RGS1 each received 3/5 votes.

Cross-site differential expression comparisons showed that all 11 hub genes were upregulated at D7 relative to D3 in the oral dataset GSE41446 (Fig. 5B). In the orthopedic reference data, CTSK was also significantly upregulated in the rat tibial D4-versus-D2 time series (log2FC = +1.90), suggesting concordant early osseointegration dynamics across sites and species. CTSK was also upregulated in the rat femoral model (log2FC = +1.69), although it did not meet the significance criteria. MMP9 and RDX were upregulated in human alveolar bone (log2FC = +3.2 and +1.4, respectively), whereas RDX showed the opposite direction in the rat femoral model (log2FC = −1.0). Other hub genes were not detectable (n.d.) on some rat platforms or had limited statistical power because of small sample sizes; their cross-site conservation therefore remains unresolved.

Classification performance was evaluated by five-fold stratified cross-validation in GSE41446 (random_state = 42; Fig. 5C). The current fixed workflow achieved an area under the receiver operating characteristic curve (AUC) of 0.960 and a Macro-F1 of 0.888. The nested approach using the full gene pool, with feature selection repeated within each training fold, achieved an AUC of 0.980 ± 0.045 and a Macro-F1 of 0.911 ± 0.145. In a further fixed-signature evaluation of the prespecified 11-gene hub signature, both AUC and Macro-F1 were 1.000 in all five outer folds, yielding AUC = 1.000 ± 0.000 and Macro-F1 = 1.000 ± 0.000. This hub-only analysis assessed the discriminative ability of a fixed signature within the same dataset without repeating feature selection in each cross-validation fold. It therefore cannot be equated with unbiased predictive performance in an independent cohort.

The classification performance of the 11 hub genes primarily reflected global time-associated transcriptional separation between D3 and D7. Even 10,000 random 11-gene signatures achieved a mean Macro-F1 of 0.724 ± 0.085 (Fig. 5D), indicating that the classification task itself lacked specificity to skeletal biology. Accordingly, the fixed-signature AUC/Macro-F1 of 1.000 represents an upper bound on in-sample separability incorporating feature-selection information, rather than evidence of independent predictive ability or specificity. The nested cross-validation AUC of 0.980 ± 0.045 is the only value in this study that can be used as an estimate of performance. Given the marked global time-associated transcriptional reprogramming in this dataset, with PC1 explaining approximately 30% of overall expression variation, these findings should be regarded as hypothesis-generating within a single cohort and cannot be directly interpreted as clinical predictive ability or independent validation.

3.5 Integration of multilevel evidence, prior functional knowledge, and cross-site conservation of hub genes

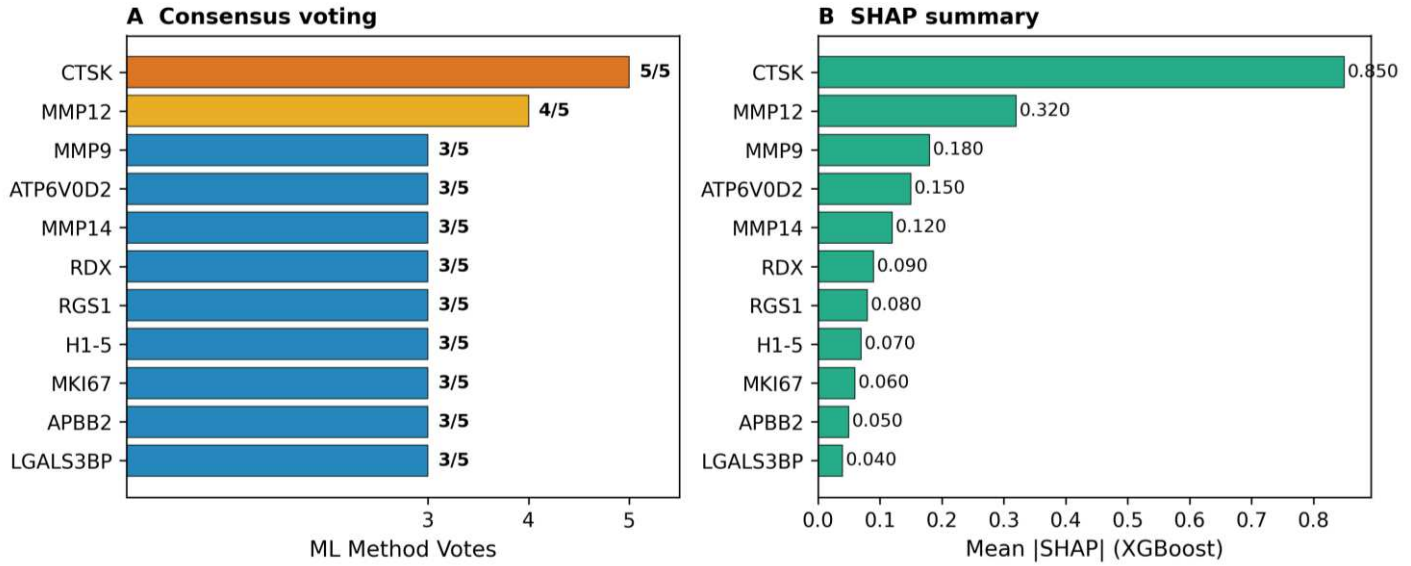

Figure 6. SHAP feature-importance analysis in human alveolar bone from D3 to D7

Table 3. Literature-based grading of bone-related functional evidence for Hub genes

Gene	Bone related function	Primary cell type	Evidence level	Key supporting reference	PMID	Direction D3 to D7
CTSK	Major osteoclast-secreted collagenase (type I collagen/bone matrix degradation); deficiency promotes alveolar bone regeneration via glycolysis-driven jaw-bone MSC osteogenesis	Osteoclast	L1	Cathepsin K deficiency promotes alveolar bone regeneration... Cell Proliferation 2021;54(8):e13058	34053135	Up
MMP9	Osteoclast gelatinase B coupling matrix resorption with angiogenic invasion and endochondral ossification; KO impairs growth-plate vascularization	Osteoclast	L1	Vu TH et al. Cell 1998;93(3):411-422	9590175	Up
MMP14	Principal osteoblast/osteocyte membrane-tethered collagenase (MT1-MMP) for pericellular type I collagen cleavage; KO causes osteopenia/skeletal dysplasia	Osteoblast/osteocyte	L1	Holmbeck K et al. Cell 1999;99(1):81-92	10520996	Up
ATP6V0D2	V-ATPase V0 d2 subunit mediating osteoclast precursor fusion and extracellular acidification/resorption; deficiency impairs fusion and increases bone mass	Osteoclast	L1	v-ATPase V0 d2-deficient mice... Nature Medicine 2006	17128270	Up
MMP12	Osteoclast-expressed metalloelastase participating in RANKL-driven bone resorption; also linked to periodontitis-related oral bone loss	Osteoclast/monocyte-macrophage lineage	L1	Hou P et al. Bone 2004;34(1):37-47	14751561	Up
RGS1	Promotes osteoclastogenesis via a super-enhancer eRNA recruiting FOXJ3 (PLC-IP3R-Ca2+ signaling)	Osteoclast precursor/immune cells	L1	Inflammation 2024 (online ahead of print; doi:10.1007	38904871	Up

	in rheumatoid arthritis			/s10753-024-02067-6)		
LGALS3BP	Secreted immunomodulatory glyco protein; bone evidence limited to t umor-exosome-driven osteoclastoge nesis (disease context)	Osteoclast lineage (disease)/immune cells	L2	Lung cancer exosomal Gal 3BP promotes osteoclastog enesis... Scientific Reports 2024	39516568	Up
RDX	ERM actin-plasma membrane linke r; osteoclast sealing-zone/ruffled-bo rder role inferred from family im munolocalization (paralog moesin has direct functional evidence)	Osteoclast (inferred)	L3	Immunolocalization of CD4 4 and the ERM family in bone cells... J Bone Miner Res 1996;11(11):1715-172 2	8915779	Up
MKI67	Canonical proliferation marker (G1 -M, absent in G0); labels prolifera ting osteoprogenitors/osteoblast-line age cells in healing bone	Proliferating cells/osteoprogenitors	L3	Scholzen T, Gerdes J. J C ell Physiol 2000;182(3):311 -322	10653597	Up
H1-5	Linker histone H1.5 (formerly HIS T1H1B); chromatin organization, c ell-cycle exit/differentiation; no dir ect bone-specific evidence found	Cycling/differentiating cells (no bone-specific context)	L3	Li JY et al. PLoS Genet 2 012;8(8):e1002879	22956909	Up
APBB2	Fe65-family adaptor (neuronal, AP P signaling); no direct bone-specifi c evidence found in systematic se arch - annotation/family inference only	Unknown (no bone evidence)	L4	The FE65 proteins and Alz heimer's disease. J Neurosc i Res 2008	17828772	Up

Abbreviations and definitions: Cell type, primary functional cell type based on the literature; L1, functional knockout or in vivo bone phenotype evidence; L2, in vitro differentiation, functional, or protein evidence without an in vivo bone phenotype under healthy physiological conditions; L3, expression or immunolocalization association, or a consensus marker; L4, no direct bone evidence, with interpretation based only on annotation or protein-family inference; H1-5, formerly HIST1H1B (linker histone H1.5; HUGO Gene Nomenclature Committee identifier HGNC:4719); Up/Down, expression direction from D3 to D7 in GSE41446 in the present study. Table-specific abbreviations: ECM, extracellular matrix; MSC, mesenchymal stem cell; KO, knockout; MT1-MMP, membrane-type 1 matrix metalloproteinase; V-ATPase, vacuolar-type H^+-ATPase; RANKL, receptor activator of nuclear factor kappa-B ligand; eRNA, enhancer RNA; FOXJ3, forkhead box J3; PLC, phospholipase C; IP3R, inositol 1,4,5-trisphosphate receptor; ERM, ezrin–radixin–moesin; APP, amyloid precursor protein; PMID, PubMed identifier.

SHAP analysis further characterized the relative contributions of hub genes to the classification models (Fig. 6). CTSK was the only feature selected by XGBoost. TreeExplainer analysis showed a strong positive association between CTSK expression and its SHAP value. SHAP values were negative in all D3 samples, indicating contributions toward a Day 3 prediction, and positive in all D7 samples, indicating contributions toward a Day 7 prediction. This pattern was consistent with the complete separation of D3 and D7 observed in the probe-level expression review, supporting CTSK as the principal discriminative feature in this classification task.

In the random forest SHAP summary incorporating all 11 hub genes, feature contributions were ranked CTSK > MMP12 > ATP6V0D2 > MMP9. This broadly agreed with the consensus voting hierarchy across machine-learning methods: CTSK with 5/5 votes, MMP12 with 4/5 votes, and most remaining genes with 3/5 votes. This concordance supports hub-gene prioritization at the level of model interpretation but should not be interpreted as independent biological evidence of causality.

To distinguish the present transcriptomic findings from established biological evidence, we reviewed the literature for each of the 11 hub genes and graded bone-related functional evidence from L1 to L4 (Table 3). CTSK, MMP9, MMP14, ATP6V0D2, and MMP12 had direct evidence of bone- or osteoclast-related function, including loss-of-

function studies or in vivo bone phenotypes (L1) [38-42]. In a rheumatoid arthritis model, RGS1 was reported to promote osteoclastogenesis through a super-enhancer-derived enhancer RNA (eRNA) that recruits FOXJ3. Because this evidence originated primarily from a single disease-context study, its generalizability should be treated cautiously despite its L1 classification [43].

Evidence linking RDX to cytoskeletal functions at the osteoclast ruffled border or sealing zone was derived mainly from ezrin–radixin–moesin (ERM) family immunolocalization and functional inference and was graded L3 [44]. MKI67 and H1-5 primarily reflected cell proliferation and chromatin state, respectively, and currently lacked direct bone-specific functional evidence; both were graded L3 [45, 46]. Bone-related evidence for LGALS3BP primarily came from a disease-context study of tumor exosome-induced osteoclastogenesis and was graded L2 [47]. No direct evidence of bone function was identified for APBB2, whose current interpretation relied mainly on gene annotation or protein-family functional inference; it was graded L4 [48].

Overall, genes among the 11 hubs with stronger direct evidence of skeletal function were concentrated in the osteoclast–ECM remodeling axis, including CTSK, the matrix metalloproteinase (MMP) family, ATP6V0D2, MMP12, and RGS1. By contrast, D3-to-D7 upregulation of APBB2, H1-5, and LGALS3BP may more plausibly reflect accompanying transcriptional changes in proliferation, chromatin remodeling, or immunomodulation and is insufficient to establish them as osseointegration-specific effector molecules. This evidence hierarchy is consistent with the interpretation that coupling between osteogenesis–ECM processes and osteoclast-mediated remodeling constitutes a conserved core program, but it does not mean that these hub genes were directly functionally validated in the present stud

4. Discussion

4.1 An immune–bone-remodeling framework for dental implant osseointegration

In bone tissue from human alveolar implant osteotomy sites, we observed coordinated D3-to-D7 upregulation of the reparative macrophage marker MRC1 and genes involved in osteogenesis–ECM processes and bone remodeling (CTSK, COL1A1, COL3A1, SPARC, LOX, MMP12, and ALPL), together with downregulation of inflammatory mediators such as TNF and IL1B. This transcriptional trajectory is consistent with a transition from an inflammation-dominated state toward repair and bone remodeling within an osteoimmunomodulatory framework [3, 19]. Its direction agrees with evidence for macrophage-mediated transitions from inflammation resolution to osteogenesis initiation in fracture healing and implantation studies [18, 20, 21], as well as macrophage-centered immune microenvironment remodeling observed at implant interfaces at single-cell resolution [24, 25]. Directional ssGSEA provided complementary support: enrichment scores for the reparative macrophage gene set increased in 19 of 22 paired samples, and the magnitude exceeded the empirical distribution of random gene sets analyzed in the same run (two-sided $P = 0.017$). The pro-inflammatory axis decreased and the pro-repair axis increased, although the magnitudes did not exceed the random envelope. Accordingly, the immune findings should be limited to directional support rather than independent gene-set-specific confirmation, because extensive global transcriptional reprogramming accompanies the D3-to-D7 interval and nominal paired tests of single-sample enrichment scores should not be interpreted in isolation [49]. The human evidence covers only D3 and D7. Longitudinal cohorts with serial sampling are needed to determine precisely when the transition begins and ends and whether it is reproducible in larger samples. The absence of adjusted significance for CD163 and IL6 also argues against generalizing these findings to a universal shift in all macrophage or inflammatory markers.

4.2 The oral osteogenic cascade: detection limitations at the transcription-factor level

At the effector-gene level, the human alveolar bone Osteogenic-ECM (red) module provided a clear and robust osteogenesis/ECM signal. At the transcription-factor level, however, RUNX2, TWIST1, SP7, and BGLAP were absent from the WGCNA input space (the 5,000 most highly variable human genes), precluding the detection of an independent module involving these genes. This absence primarily reflects an inherent consequence of a network design conditioned on highly variable gene filtering, rather than evidence that osteogenic

transcriptional activity is absent [50]. Transcription factors in the mixed-cell system represented by implant osteotomy bone chips generally have low expression and limited between-sample variation, making them susceptible to exclusion by variance filtering. Bulk signals from bone chips are dominated by stromal and immune cells, further diluting transcription-factor dynamics within osteoprogenitor subsets [51]. The narrow D3-to-D7 interval and microarray probe sensitivity may also limit detection of low-abundance transcripts. In contrast, RobustRankAggreg, which does not depend on highly variable gene prefiltering, identified significant signals in 11 of 12 prespecified key osteogenic genes, including RUNX2, BMP2, SP7, TWIST1, BGLAP, and ALPL; only CTGF was not significant ($P = 0.232$). This suggests directionally concordant signals for these transcription factors during D3–D7 at the level of cross-dataset rankings, while their magnitudes and co-expression structures remain insufficient for module-level conclusions [52]. The lack of significance for BMP2 in the human oral data also precludes a claim that the complete "BMP2 → RUNX2 → ALPL" osteogenic cascade was reproduced in human alveolar bone [53]. Co-expression evidence arose mainly from rat modules; validation in human alveolar bone still requires deeper RNA-seq, single-cell or spatial transcriptomics, and direct functional perturbation experiments. These limitations at the transcription-factor level do not weaken the effector-gene conclusions, because identification and cross-species preservation of the Osteogenic-ECM module are independent of whether transcription factors entered the highly variable gene list.

4.3 A conserved core coupling osteogenesis–ECM processes with osteoclast-mediated matrix remodeling: directionally concordant molecular signals between oral and long bones

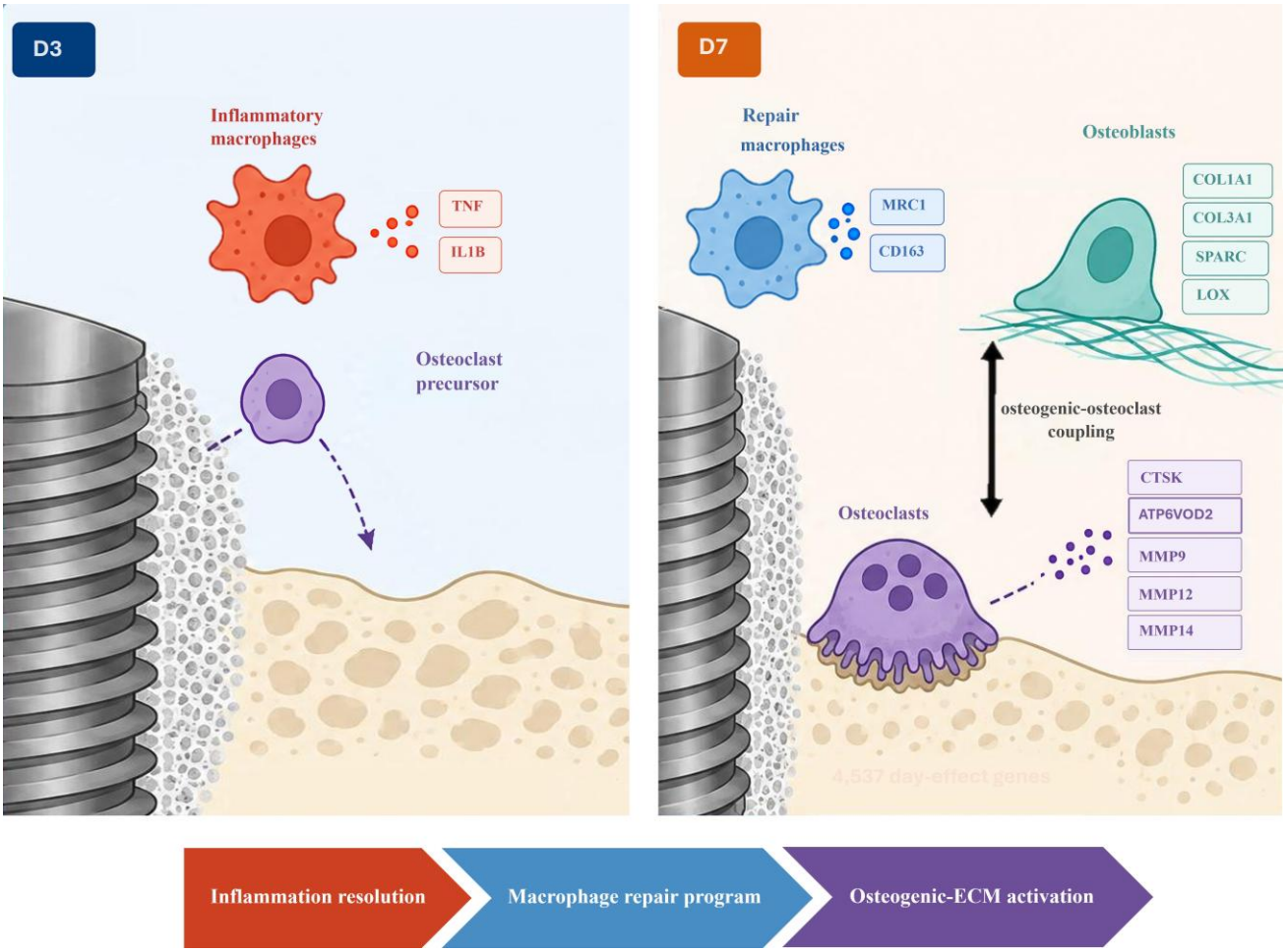

Figure 7. Immune-to-bone-remodeling transition at D3–D7 and the osteogenic–osteoclast coupling core in human alveolar bone: an integrative schematic.

Through site stratification and statistical tests of conservation, this study assembled mutually corroborating rather than redundant evidence from three analytical approaches: differential expression classification, co-expression networks, and machine learning. The 42 conserved genes that were significant and directionally concordant in both oral and orthopedic strata showed strong enrichment for osteogenesis (FE = 73.3, P = 7.1×10^{-13}). Of the 159 genes in the human WGCNA red module, 113 were detectable on the same rat platform, and 73 of these (64.6% of detectable genes) belonged to the best-matching rat module, significantly exceeding the random baseline of 34.2% (hypergeometric P = 1.77×10^{-11}). The modulePreservation analysis also indicated strong preservation (Zsummary = 13.31). CTSK, the consensus machine-learning hub with 5/5 votes, was significantly upregulated in both human alveolar bone and the early rat tibial time series. Together, these lines of evidence suggest that a core program coupling osteogenesis–ECM deposition with osteoclast-mediated matrix remodeling is likely a shared basis of osseointegration across sites and species, rather than a feature unique to orthopedic models or an artifact of the analytical workflow [54, 55] (Fig. 7). This conserved core further suggests that interventions targeting ECM remodeling (CTSK/LOX/SPARC/COL1A1) and osteoclast–

remodeling coupling (CTSK/ATP6V0D2/MMP9) may have relevance across anatomical sites. Nevertheless, the observed conservation is statistical, involving differential expression direction and co-expression structure; it does not establish functional conservation or causality. In addition, cross-site classification pooled temporal, loading, and treatment comparisons, making the results more appropriate as descriptive evidence than as estimates of effect sizes under an identical biological stimulus.

4.4 Alveolar bone-specific features of osseointegration

In contrast to the clear functional enrichment of conserved programs, the 4,359 Oral-specific genes showed no reproducible enrichment in curated osteogenesis, ECM, remodeling, or immune gene sets. Their most prominent functional annotations involved fundamental metabolic processes, including translation, oxidative phosphorylation, the TCA cycle, and mitochondrial ATP synthesis. This pattern may more plausibly reflect the demands for protein synthesis and energy metabolism accompanying global D3-to-D7 transcriptional reprogramming than an alveolar bone-specific regulatory pathway for osseointegration [56]. The marked difference in the numbers of Oral-specific and Ortho-specific genes (4,359 versus 436) may also arise partly from asymmetries in sample size, statistical power, and comparison type between the two strata, and cannot yet be used to estimate the true extent of site-related biological differences [57]. Furthermore, alveolar bone-chip samples generally contain higher proportions of marrow, soft tissue, and immune cells than cortical bone specimens, so oral-specific signals may also be driven by differences in tissue composition [58]. Taken together, the current findings do not support interpreting Oral-specific genes as a distinct alveolar bone-specific "osseointegration pathway." Defining genuine site-specific programs will require matched comparison types, such as paired oral–long-bone designs under identical treatment or loading conditions, more homogeneous sampling strategies, and larger human sample sizes.

4.5 Clinical translation: oral-specific biomarkers and implant surface design

If the D3-to-D7 immune-to-bone-remodeling transition is reproduced in larger cohorts, this interval may provide a candidate molecular window for monitoring early implant osseointegration. Among candidate biomarkers, CTSK currently has the most complete chain of supporting evidence. It showed the largest D7 increase among the osteogenesis–ECM/remodeling key genes examined in human alveolar bone (log2FC = +3.66), its signal was confirmed by probe-level review, and it was also significantly upregulated in the early rat tibial time series. Cathepsin K can be assessed using clinically accessible platforms, including serum or gingival

crevicular fluid enzyme-linked immunosorbent assays (ELISAs) and quantitative polymerase chain reaction (qPCR), providing basic measurability as a candidate process biomarker of early osseointegration [59]. MMP family members (MMP9/MMP12/MMP14) and the osteoclast acidification subunit ATP6V0D2 belong to the same osteoclast–ECM remodeling coupling program identified here and have similar priority as candidates [60]. By contrast, the inconsistent direction of RDX across sites suggests limited value as a general cross-site biomarker. These judgments, however, derive entirely from in-sample analyses of a single human cohort and do not establish cross-cohort prediction or clinical diagnostic ability. Associations between candidate biomarkers and osseointegration outcomes, such as bone-to-implant contact, stability, and long-term implant survival, must be established in independent prospective cohorts before incorporation into clinical decision-making [61].

4.6 Evidence from independent external validation

In the absence of an independent human alveolar bone transcriptomic cohort, external validation was limited to three complementary but individually incomplete levels, with the evidential boundaries of each explicitly defined. At the level of published human samples, two qPCR studies in human jaw bone examined osteogenesis-related genes, including ALPL, BMP2, COL1A1, RUNX2, osteocalcin (OCN), osteoprotegerin (OPG), and receptor activator of nuclear factor kappa-B ligand (RANKL), in implant-adherent cells and at nanopatterned implant interfaces, respectively, and reported upregulation during early healing [62, 63]. Although these genes do not fully overlap with the present 11-hub-gene panel, COL1A1, ALPL, BMP2, and RUNX2 are key members of the conserved osteogenesis–ECM program examined here. Their reported upregulation agrees with the direction of the present D3-to-D7 findings, providing qPCR support from independent patient samples for activation of early osteogenic programs in human alveolar bone. The two qPCR studies shared authors and belonged to the Gothenburg bone biomaterials research network; they should therefore be regarded as two complementary measurements within that network, rather than two fully independent external validations. Their authors were not members of the Cooper/Thalji/Nares team responsible for the discovery cohort GSE41446. Thus, independence at the patient and institutional levels is supported, whereas twofold independence at the research-network level is not. The present findings also agree directionally with earlier human molecular assessments published by the discovery cohort's research team [26, 64]. Such

concordance constitutes within-cohort reproducibility evidence and is not counted as independent external validation [65].

At the functional and protein levels, cathepsin K has an established experimental basis: CTSK encodes a major osteoclast-secreted collagenase responsible for degrading type I collagen and other bone matrix proteins and is a marker of bone resorption and remodeling [38]. Studies in CTSK-deficient mice have also shown that its loss promotes proliferation and osteogenic differentiation of jaw bone marrow mesenchymal stem cells through glycolysis and enhances alveolar bone regeneration [38], suggesting bidirectional, pro-resorptive and pro-osteogenic roles across cell types and biological contexts. This duality is important for interpreting the D7 increase observed here. D3-to-D7 upregulation of CTSK may more plausibly reflect increased matrix clearance and remodeling during the initiation of osteoclast–osteoblast coupling at the implant interface; interpreting CTSK expression exclusively as an indicator of either bone resorption or bone formation may therefore be incomplete [55]. These functional and protein findings come from independent experimental literature, rather than direct measurements in this study, and serve only as mechanistic background. Public expression resources such as the Human Protein Atlas (HPA) and Genotype-Tissue Expression (GTEx) project do not include human bone tissue samples, and their bulk signals are insensitive to minor cell populations such as osteoclasts; these resources were therefore not included in the validation framework. Overall, external validation in this study comprises three partial levels: cross-species transcriptomic conservation in rat tibia, published human jaw bone qPCR support, and established functional/protein literature on CTSK. Direct transcriptomic validation in an independent human alveolar bone cohort and protein quantification of hub genes remain the principal methodological gaps.

4.7 Clinical and materials science implications

On the clinical timeline, the D3-to-D7 immune-to-bone-remodeling transition broadly aligns with early postoperative healing: the first week corresponds to acute inflammation and clot remodeling, consistent with the D3 inflammatory program, whereas the second to third weeks correspond to initiation of the osteogenesis–ECM program, consistent with the D7 osteogenic state [66]. If this correspondence holds and molecular monitoring is feasible, D3–D7 may represent a candidate window for monitoring early osseointegration. Conventional time points for early loading decisions and stability assessments, at 4–6 and 12 weeks after surgery, occur substantially later than the molecular transition observed here [67]. However, the study covers only D3 and D7.

Molecular trajectories of mineralization, bone maturation, and homeostatic maintenance after D7 are extrapolations, and the present findings do not provide sufficient evidence to adjust clinical protocols [68].

Regarding the measurability of candidate monitoring biomarkers, cathepsin K can be assessed using serum/gingival crevicular fluid ELISA, qPCR, and microarray platforms, providing a practical basis for its consideration as a candidate process biomarker of early osseointegration [59]. MMP9/MMP12/MMP14 and ATP6V0D2 belong to the same osteoclast–ECM remodeling coupling program and have similar measurability and priority. Measurability, however, does not establish an association with osseointegration outcomes; such associations must be demonstrated prospectively in independent human cohorts.

For the design of osteoimmunomodulatory implant surfaces, the current evidence more strongly supports identifying candidate targets within conserved programs of osteogenesis–ECM deposition and osteoclast–remodeling coupling than targeting oral-specific pathways that remain poorly characterized. Directions for exploration include surface features that maintain the temporal balance between ECM remodeling and osteoclast activity, host-response monitoring strategies using CTSK/MMP-related signals as readouts, and local regulation that promotes the early transition from inflammation resolution to osteogenesis [3, 18]. These approaches require validation in in vivo models and preclinical studies before translational development.

4.8 Limitations

The conclusions should be interpreted within an explicit hierarchy of evidence. Limitations concern four areas: the data foundation, temporal resolution, cross-site comparison methods, and validation level. First, the Core Discovery stratum contained only two oral bone datasets, with human evidence restricted to a single cohort, GSE41446 (44 samples, 11 participants, two implant surfaces, and D3/D7). Second, temporal resolution and tissue composition impose limitations. GSE41446 covers only D3 and D7 and lacks human data from the earlier acute inflammatory phase (24–72 h after surgery) and the bone maturation/homeostatic phase. The exact onset and completion of the immune-to-osteogenic transition, temporal modulation of surface effects, and mineralization trajectories after D7 therefore cannot be defined. Third, cross-site comparisons have methodological limitations. Oral and orthopedic datasets differ in comparison type (time series, loading, and treatment/ablation), platform (microarray and RNA-seq), species, and sample size. Cross-site classification can therefore serve only as a descriptive comparison, not as an estimate of effects under an identical biological stimulus. Finally, the validation level is limited. Cross-site conservation of hub genes was evaluated in rat rather

than human bone tissue, and its cross-site relevance requires testing in independent human bone cohorts. Published human qPCR panels mainly cover osteogenic markers and do not directly include CTSK or MMP family members. Direct qPCR or protein-level validation of the hub genes remains unavailable.

5. Conclusions

Using a site-stratified strategy to integrate oral and orthopedic osseointegration transcriptomes, this study reached the following conclusions concerning the three questions posed in the Introduction.

1. Human alveolar bone exhibits a directionally concordant immune-to-bone-remodeling transition from D3 to D7. The reparative macrophage marker MRC1 is upregulated, whereas TNF and IL1B are downregulated, alongside coordinated upregulation of genes involved in osteogenesis–ECM processes and osteoclast-mediated matrix remodeling, including CTSK, COL1A1, COL3A1, SPARC, LOX, MMP12, and ALPL. Paired participant-by-surface testing supports this direction of transition, with MRC1 enrichment scores increasing in 19 of 22 paired samples (empirical $P = 0.017$).

2. The core program coupling osteogenesis–ECM processes with osteoclast-mediated matrix remodeling is directionally concordant between oral and orthopedic datasets. The 42 directionally concordant conserved genes show significant enrichment for osteogenesis (FE = 73.3, $P = 7.1 \times 10^{-13}$). Preservation of the human WGCNA red module on the rat platform significantly exceeds the random baseline (64.6% versus 34.2%; hypergeometric $P = 1.77 \times 10^{-11}$; modulePreservation Zsummary = 13.31), suggesting a shared core of osteoblast–osteoclast coupling across sites and species.

3. Among the 11 hub genes identified by consensus machine-learning selection, only CTSK shows conserved upregulation across both sites and species and can be prioritized as a candidate process biomarker for validation. The remaining hub genes currently remain oral-specific candidates. In contrast, Oral-specific gene enrichment is concentrated in translation and mitochondrial energy metabolism, without reproducible enrichment for osteogenesis, ECM, remodeling, or immunity. This pattern more plausibly reflects global D3-to-D7 transcriptional reprogramming and is insufficient to define a distinct oral-specific osseointegration pathway.

Declarations

The authors received no funding for this study.

Ethics, Consent to Participate, and Consent to Publish declarations: not applicable.

Clinical trial number: not applicable.

Data availability

The datasets generated during and/or analysed during the current study are available in the NCBI Gene Expression Omnibus (GEO) repository,

https://www.ncbi.nlm.nih.gov/geo/query/acc.cgi?acc=GSE41446;

https://www.ncbi.nlm.nih.gov/geo/query/acc.cgi?acc=GSE304968;

https://www.ncbi.nlm.nih.gov/geo/query/acc.cgi?acc=GSE35976;

https://www.ncbi.nlm.nih.gov/geo/query/acc.cgi?acc=GSE54294;

https://www.ncbi.nlm.nih.gov/geo/query/acc.cgi?acc=GSE113520;

https://www.ncbi.nlm.nih.gov/geo/query/acc.cgi?acc=GSE227869 [69-74].

References

1. Branemark P-I. Osseointegration and its experimental background. The Journal of Prosthetic Dentistry. 1983;50(3):399-410. https://doi.org/10.1016/S0022-3913(83)80101-2
2. Bai L, Chen P, Zhao Y, Hang R, Yao X, Tang B, et al. A micro/nano-biomimetic coating on titanium orchestrates osteo/angio-genesis and osteoimmunomodulation for advanced osseointegration. Biomaterials. 2021;278:121162. https://doi.org/10.1016/j.biomaterials.2021.121162
3. Chen Z, Bachhuka A, Wei F, Wang X, Liu G, Vasilev K, et al. Nanotopography-based strategy for the precise manipulation of osteoimmunomodulation in bone regeneration. Nanoscale. 2017;9(46):18129-52. https://doi.org/10.1039/c7nr05913b
4. Kondo T, Yamada M, Egusa H. Innate immune regulation in dental implant osseointegration. Journal of prosthodontic research. 2024;68(4):511-21. https://doi.org/10.2186/jpr.JPR_D_23_00198
5. Shirazi S, Ravindran S, Cooper LF. Topography-mediated immunomodulation in osseointegration; Ally or Enemy. Biomaterials. 2022;291:121903. https://doi.org/10.1016/j.biomaterials.2022.121903
6. Souza JGS, Nagay BE, Martins R, Bertolini M, Shibli JA, Aparicio C, et al. Engineered surface strategies to manage dental implant-related infections. Periodontol 2000. 2025;n/a(n/a). https://doi.org/10.1111/prd.12637
7. Monje A, Salvi GE. Diagnostic methods/parameters to monitor peri-implant conditions. Periodontol 2000. 2024;95(1):20-39. https://doi.org/10.1111/prd.12584
8. Berglundh T, Mombelli A, Schwarz F, Derks J. Etiology, pathogenesis and treatment of peri-implantitis: A European perspective. Periodontol 2000. 2024. https://doi.org/10.1111/prd.12549
9. de Campos Kajimoto N, de Paiva Buischi Y, Mohamadzadeh M, Loomer P. The Oral Microbiome of Peri-Implant Health and Disease: A Narrative Review. Dentistry journal. 2024;12(10). https://doi.org/10.3390/dj12100299
10. Smeriglio P, Zalc A. Cranial Neural Crest Cells Contribution to Craniofacial Bone Development and Regeneration. Current Osteoporosis Reports. 2023;21(5):624-31. https://doi.org/10.1007/s11914-023-00804-8
11. Hu K, Olsen BR. Osteoblast-derived VEGF regulates osteoblast differentiation and bone formation during bone repair. The Journal of clinical investigation. 2016;126(2):509-26. https://doi.org/10.1172/jci82585
12. Ono T, Nakashima T. Oral bone biology. Journal of oral biosciences. 2022;64(1):8-17. https://doi.org/10.1016/j.job.2022.01.008
13. Bressan E, Guazzo R, Tomasi C, Peña TG, Galindo-Moreno P, Caponio VCA, et al. Influence of soft tissue thickness on marginal bone level around dental implants: A systematic review with meta-analysis and trial-sequential analysis. Clin Oral Implants Res. 2023;34(5):405-15. https://doi.org/10.1111/clr.14032

14. Al Zahrani S, Al Mutairi AA. Crestal Bone Loss Around Submerged and Non-Submerged Dental Implants in Individuals with Type-2 Diabetes Mellitus: A 7-Year Prospective Clinical Study. Medical principles and practice : international journal of the Kuwait University, Health Science Centre. 2019;28(1):75-81. https://doi.org/10.1159/000495111
15. Buser D, Broggini N, Wieland M, Schenk RK, Denzer AJ, Cochran DL, et al. Enhanced Bone Apposition to a Chemically Modified SLA Titanium Surface. J Dent Res. 2004;83(7):529-33. https://doi.org/10.1177/154405910408300704
16. Ji Z, Wan Y, Wang H, Yu M, Zhao Z, Wang T, et al. Effects of surface morphology and composition of titanium implants on osteogenesis and inflammatory responses: a review. Biomedical materials (Bristol, England). 2023;18(4). https://doi.org/10.1088/1748-605X/acd976
17. Wu M, Wu S, Chen W, Li YP. The roles and regulatory mechanisms of TGF-β and BMP signaling in bone and cartilage development, homeostasis and disease. Cell research. 2024;34(2):101-23. https://doi.org/10.1038/s41422-023-00918-9
18. Hachemi Y, Perrin S, Ethel M, Julien A, Vettese J, Geisler B, et al. Multimodal analyses of immune cells during bone repair identify macrophages as a therapeutic target in musculoskeletal trauma. Bone research. 2024;12(1):56. https://doi.org/10.1038/s41413-024-00347-3
19. Takayanagi H. Osteoimmunology: shared mechanisms and crosstalk between the immune and bone systems. Nature reviews Immunology. 2007;7(4):292-304. https://doi.org/10.1038/nri2062
20. Schlundt C, El Khassawna T, Serra A, Dienelt A, Wendler S, Schell H, et al. Macrophages in bone fracture healing: Their essential role in endochondral ossification. Bone. 2018;106:78-89. https://doi.org/10.1016/j.bone.2015.10.019
21. Raggatt LJ, Wullschleger ME, Alexander KA, Wu ACK, Millard SM, Kaur S, et al. Fracture Healing via Periosteal Callus Formation Requires Macrophages for Both Initiation and Progression of Early Endochondral Ossification. The American Journal of Pathology. 2014;184(12):3192-204. https://doi.org/10.1016/j.ajpath.2014.08.017
22. Okamoto K. Crosstalk between bone and the immune system. Journal of bone and mineral metabolism. 2024;42(4):470-80. https://doi.org/10.1007/s00774-024-01539-x
23. Chen G, Deng C, Li YP. TGF-β and BMP signaling in osteoblast differentiation and bone formation. International journal of biological sciences. 2012;8(2):272-88. https://doi.org/10.7150/ijbs.2929
24. Zhou J, Liang H, Chen J, Li A, Dai J, Li P. Macrophage-related immune responses to polyetherketoneketone bone implants: Single-cell transcriptome analysis. Materials today Bio. 2025;35:102257. https://doi.org/10.1016/j.mtbio.2025.102257
25. Zhou J, Li A, Chen J, Dai J, Zhang W, Yang Z, et al. Mapping Immune-Inflammatory Niches on Zirconia Bone Implants: Single-Cell Transcriptomic Profiling. Research.9:1162. https://doi.org/10.34133/research.1162
26. Thalji GN, Nares S, Cooper LF. Early molecular assessment of osseointegration in humans. Clin Oral Implan Res. 2014;25(11):1273-85. https://doi.org/10.1111/clr.12266
27. Donos N, Hamlet S, Lang NP, Salvi GE, Huynh-Ba G, Bosshardt DD, et al. Gene expression profile of osseointegration of a hydrophilic compared with a hydrophobic microrough implant surface. Clin Oral Implan Res. 2011;22(4):365-72. https://doi.org/10.1111/j.1600-0501.2010.02113.x
28. Page MJ, McKenzie JE, Bossuyt PM, Boutron I, Hoffmann TC, Mulrow CD, et al. The PRISMA 2020 statement: an updated guideline for reporting systematic reviews. BMJ. 2021;372:n71. https://doi.org/10.1136/bmj.n71
29. Wu Y, Wang F, He Y, Zhang Y, Zeng Y, Zheng F, et al. A biomechanical optimized Zr58Cu25Al14Nb3 bulk metallic glass dental implant improves peri-implant stress distribution and bone quality under physiological loading. BMEMat. 2026;n/a(n/a):e70116. https://doi.org/10.1002/bmm2.70116
30. Suhardi VJ, Oktarina A, Hammad M, Niu Y, Li Q, Thomson A, et al. Prevention and treatment of peri-implant fibrosis by functionally inhibiting skeletal cells expressing the leptin receptor. Nature biomedical engineering. 2024;8(10):1285-307. https://doi.org/10.1038/s41551-024-01238-y
31. Thalji G, Gretzer C, Cooper LF. Comparative molecular assessment of early osseointegration in implant-adherent cells. Bone. 2013;52(1):444-53. https://doi.org/10.1016/j.bone.2012.07.026
32. Thorfve A, Bergstrand A, Ekström K, Lindahl A, Thomsen P, Larsson A, et al. Gene expression profiling of peri-implant healing of PLGA-Li+ implants suggests an activated Wnt signaling pathway in vivo. PloS one. 2014;9(7):e102597. https://doi.org/10.1371/journal.pone.0102597
33. Langfelder P, Horvath S. WGCNA: an R package for weighted correlation network analysis. BMC Bioinformatics. 2008;9(1):559. https://doi.org/10.1186/1471-2105-9-559
34. Langfelder P, Luo R, Oldham MC, Horvath S. Is my network module preserved and reproducible? PLoS computational biology. 2011;7(1):e1001057. https://doi.org/10.1371/journal.pcbi.1001057
35. Kolde R, Laur S, Adler P, Vilo J. Robust rank aggregation for gene list integration and meta-analysis. Bioinformatics. 2012;28(4):573-80. https://doi.org/10.1093/bioinformatics/btr709
36. Benjamini Y, Hochberg Y. Controlling the False Discovery Rate: A Practical and Powerful Approach to Multiple Testing. Journal of the Royal Statistical Society: Series B (Methodological). 1995;57(1):289-300. https://doi.org/10.1111/j.2517-6161.1995.tb02031.x
37. Leek JT, Johnson WE, Parker HS, Jaffe AE, Storey JD. The sva package for removing batch effects and other unwanted variation in high-throughput experiments. Bioinformatics. 2012;28(6):882-3. https://doi.org/10.1093/bioinformatics/bts034

38. Zhang W, Dong Z, Li D, Li B, Liu Y, Zheng X, et al. Cathepsin K deficiency promotes alveolar bone regeneration by promoting jaw bone marrow mesenchymal stem cells proliferation and differentiation via glycolysis pathway. Cell proliferation. 2021;54(7):e13058. https://doi.org/10.1111/cpr.13058
39. Vu TH, Shipley JM, Bergers G, Berger JE, Helms JA, Hanahan D, et al. MMP-9/gelatinase B is a key regulator of growth plate angiogenesis and apoptosis of hypertrophic chondrocytes. Cell. 1998;93(3):411-22. https://doi.org/10.1016/s0092-8674(00)81169-1
40. Holmbeck K, Bianco P, Caterina J, Yamada S, Kromer M, Kuznetsov SA, et al. MT1-MMP-Deficient Mice Develop Dwarfism, Osteopenia, Arthritis, and Connective Tissue Disease due to Inadequate Collagen Turnover. Cell. 1999;99(1):81-92. https://doi.org/10.1016/S0092-8674(00)80064-1
41. Lee S-H, Rho J, Jeong D, Sul J-Y, Kim T, Kim N, et al. v-ATPase V0 subunit d2–deficient mice exhibit impaired osteoclast fusion and increased bone formation. Nature Medicine. 2006;12(12):1403-9. https://doi.org/10.1038/nm1514
42. Hou P, Troen T, Ovejero MC, Kirkegaard T, Andersen TL, Byrjalsen I, et al. Matrix metalloproteinase-12 (MMP-12) in osteoclasts: new lesson on the involvement of MMPs in bone resorption. Bone. 2004;34(1):37-47. https://doi.org/10.1016/j.bone.2003.08.011
43. Yuan L, Jiang N, Li Y, Wang X, Wang W. RGS1 Enhancer RNA Promotes Gene Transcription by Recruiting Transcription Factor FOXJ3 and Facilitates Osteoclastogenesis Through PLC-IP3R-dependent Ca2+ Response in Rheumatoid Arthritis. Inflammation. 2025;48(1):447-63. https://doi.org/10.1007/s10753-024-02067-6
44. Nakamura H, Ozawa H. Immunolocalization of CD44 and the ERM family in bone cells of mouse tibiae. Journal of Bone and Mineral Research. 1996;11(11):1715-22. https://doi.org/10.1002/jbmr.5650111115
45. Scholzen T, Gerdes J. The Ki-67 protein: From the known and the unknown. Journal of Cellular Physiology. 2000;182(3):311-22. https://doi.org/10.1002/(SICI)1097-4652(200003)182:3<311::AID-JCP1>3.0.CO;2-9
46. Li J-Y, Patterson M, Mikkola HKA, Lowry WE, Kurdistani SK. Dynamic Distribution of Linker Histone H1.5 in Cellular Differentiation. PLOS Genetics. 2012;8(8):e1002879. https://doi.org/10.1371/journal.pgen.1002879
47. Ghanta P, Hessel E, Arias-Alvarado A, Aghayev M, Ilchenko S, Kasumov T, et al. Lung cancer exosomal Gal3BP promotes osteoclastogenesis with potential connotation in osteolytic metastasis. Sci Rep. 2024;14(1):27201. https://doi.org/10.1038/s41598-024-79006-w
48. McLoughlin DM, Miller CCJ. The FE65 proteins and Alzheimer's disease. Journal of Neuroscience Research. 2008;86(4):744-54. https://doi.org/10.1002/jnr.21532
49. Murray PJ, Allen JE, Biswas SK, Fisher EA, Gilroy DW, Goerdt S, et al. Macrophage activation and polarization: nomenclature and experimental guidelines. Immunity. 2014;41(1):14-20. https://doi.org/10.1016/j.immuni.2014.06.008
50. Ranek JS, Stallaert W, Milner JJ, Redick M, Wolff SC, Beltran AS, et al. DELVE: feature selection for preserving biological trajectories in single-cell data. Nature Communications. 2024;15(1):2765. https://doi.org/10.1038/s41467-024-46773-z
51. Meng G, Tang W, Huang E, Li Z, Feng H. A comprehensive assessment of cell type-specific differential expression methods in bulk data. Briefings in Bioinformatics. 2023;24(1):bbac516. https://doi.org/10.1093/bib/bbac516
52. Morabito S, Reese F, Rahimzadeh N, Miyoshi E, Swarup V. hdWGCNA identifies co-expression networks in high-dimensional transcriptomics data. Cell Reports Methods. 2023;3(6). https://doi.org/10.1016/j.crmeth.2023.100498
53. Valat A, Fourel L, Sales A, Machillot P, Bouin A-P, Fournier C, et al. Interplay between integrins and cadherins to control bone differentiation upon BMP-2 stimulation. 2023;Volume 10 - 2022. https://doi.org/10.3389/fcell.2022.1027334
54. Tang Y, Wu X, Lei W, Pang L, Wan C, Shi Z, et al. TGF-beta1-induced migration of bone mesenchymal stem cells couples bone resorption with formation. Nat Med. 2009;15(7):757-65. https://doi.org/10.1038/nm.1979
55. Sims NA. Osteoclast-derived coupling factors: origins and state-of-play Louis V Avioli lecture, ASBMR 2023. Journal of bone and mineral research : the official journal of the American Society for Bone and Mineral Research. 2024;39(10):1377-85. https://doi.org/10.1093/jbmr/zjae110
56. Nandy A, Helderman RCM, Thapa S, Jayapalan S, Richards A, Narayani N, et al. Lipolysis supports bone formation by providing osteoblasts with endogenous fatty acid substrates to maintain bioenergetic status. Bone research. 2023;11(1):62. https://doi.org/10.1038/s41413-023-00297-2
57. Goll JB, Bosinger SE, Jensen TL, Walum H, Grimes T, Tharp GK, et al. The Vacc-SeqQC project: Benchmarking RNA-Seq for clinical vaccine studies. 2023;Volume 13 - 2022. https://doi.org/10.3389/fimmu.2022.1093242
58. Chu T, Wang Z, Pe'er D, Danko CG. Cell type and gene expression deconvolution with BayesPrism enables Bayesian integrative analysis across bulk and single-cell RNA sequencing in oncology. Nature Cancer. 2022;3(4):505-17. https://doi.org/10.1038/s43018-022-00356-3
59. Bayırlı AB, Uytun M, Saruhan E, Kırlı İ, Öztürk A. Association of serum 25(OH)D with Cathepsin K levels in gingival crevicular fluid and saliva in periodontal health and disease: a cross-sectional study. BMC Oral Health. 2026;26(1):237. https://doi.org/10.1186/s12903-025-07637-0
60. Barsony J, Xu Q, Verbalis JG. Hyponatremia elicits gene expression changes driving osteoclast differentiation and functions. Molecular and Cellular Endocrinology. 2022;554:111724. https://doi.org/10.1016/j.mce.2022.111724
61. Riley RD, Archer L, Snell KIE, Ensor J, Dhiman P, Martin GP, et al. Evaluation of clinical prediction models (part 2): how to undertake an external validation study. BMJ. 2024;384:e074820. https://doi.org/10.1136/bmj-2023-074820

62. Sayardoust S, Omar O, Norderyd O, Thomsen P. Implant-associated gene expression in the jaw bone of smokers and nonsmokers: A human study using quantitative qPCR. Clin Oral Implan Res. 2018;29(9):937-53. https://doi.org/10.1111/clr.13351
63. Karazisis D, Omar O, Petronis S, Thomsen P, Rasmusson L. Molecular Response to Nanopatterned Implants in the Human Jaw Bone. ACS biomaterials science & engineering. 2021;7(12):5878-89. https://doi.org/10.1021/acsbiomaterials.1c00861
64. Thalji G, Cooper LF. Molecular assessment of osseointegration in vitro: a review of current literature. Int J Oral Maxillofac Implants. 2014;29(2):e171-99. https://doi.org/10.11607/jomi.te55
65. Gallitto G, Englert R, Kincses B, Kotikalapudi R, Li J, Hoffschlag K, et al. External validation of machine learning models—registered models and adaptive sample splitting. GigaScience. 2025;14:giaf036. https://doi.org/10.1093/gigascience/giaf036
66. Wang F, Lin W, Liu L, Chen W, Wu L, Song W, et al. Titanium-guided neutrophil dynamics for inflammation resolution and tissue integration. Biomaterials. 2026;330:124048. https://doi.org/10.1016/j.biomaterials.2026.124048
67. Botros KH, Adel-Khattab D, Eldabe AK, Abuel Ela HA. Early versus conventional loading for fully guided immediate implant placement in molar sites: a randomized controlled clinical study. Int J Implant Dent. 2025;11(1):39. https://doi.org/10.1186/s40729-025-00624-8
68. Feng X, Wang H, Weng Y, Chen Y, Huang J, Wang Z. Paired-Related Homeobox 1-Positive Cells Are Needed for Osseointegration. Int J Oral Maxillofac Implants. 2024;39(6):893-903. https://doi.org/10.11607/jomi.10852
69. Cooper LF, Thalji GN, Nares S. Early molecular assessment of osseointegration in humans [dataset]. NCBI Gene Expression Omnibus. 2013. GSE41446. https://www.ncbi.nlm.nih.gov/geo/query/acc.cgi?acc=GSE41446
70. Wu Y, Wang F, He Y, Chen K, Sun B, Sun Y. Lower Elastic Modulus of Novel Zr58Cu25Al14Nb3 Dental Implants Improves Stress Distribution and Osteogenesis in Peri-implant Alveolar Bone Under Physiological Loading [dataset]. NCBI Gene Expression Omnibus. 2025. GSE304968. https://www.ncbi.nlm.nih.gov/geo/query/acc.cgi?acc=GSE304968
71. Cooper LF, Thalji GN. Genome wide array analysis of endosseous implant adherent cellular phenotypes [dataset]. NCBI Gene Expression Omnibus. 2012. GSE35976. https://www.ncbi.nlm.nih.gov/geo/query/acc.cgi?acc=GSE35976
72. Thorfve A, Tengvall P. Gene Expression Profiling of Peri-implant Healing of PLGA-Li+ Implants Suggests an Activated Wnt Signaling Pathway in vivo [dataset]. NCBI Gene Expression Omnibus. 2014. GSE54294. https://www.ncbi.nlm.nih.gov/geo/query/acc.cgi?acc=GSE54294
73. Dong X, Lan J. Co-expression Networks of mRNAs and non-coding RNAs of bones around implants in hyperlipidemic rats (RNA-seq data sets) [dataset]. NCBI Gene Expression Omnibus. 2021. GSE113520. https://www.ncbi.nlm.nih.gov/geo/query/acc.cgi?acc=GSE113520
74. Vincentius S, David O, Yurii C. Transcriptomic profile of Lin negative, LEPR positive cells of murine peri-implant fibrous tissue and peri-implant bone [dataset]. NCBI Gene Expression Omnibus. 2024. GSE227869. https://www.ncbi.nlm.nih.gov/geo/query/acc.cgi?acc=GSE227869